GGFlow: A Graph Flow Matching Method with Efficient Optimal Transport

Xiaoyang Hou[*] *houxiaoyang22s@ict.ac.cn*
Institute of Computing Technology
University of the Chinese Academy of Sciences
Tian Zhu[*] *zhutian22s@ict.ac.cn*
Institute of Computing Technology
University of the Chinese Academy of Sciences
Milong Ren *renmilong21b@ict.ac.cn*
Institute of Computing Technology
University of the Chinese Academy of Sciences
Dongbo Bu *dbu@ict.ac.cn*
Institute of Computing Technology
University of the Chinese Academy of Sciences
Central China Research Institute for Artificial Intelligence Technologies
Chunming Zhang *zhangchunming@ncic.ac.cn*
Institute of Computing Technology
Western Institute of Computing Technology
Phil Rivers Technology
Xin Gao [†] *xin.gao@kaust.edu.sa*
King Abdullah University of Science and Technology
Shiwei Sun [†] *dwsun@ict.ac.cn*
Institute of Computing Technology
University of the Chinese Academy of Sciences
Western Institute of Computing Technology

Reviewed on OpenReview: *https://openreview.net/forum?id=K8RlXtMgzo*

Abstract

Generating graph-structured data is crucial in various domains but remains challenging due to the complex interdependencies between nodes and edges. To enhance generation performance, we propose GGFlow, a discrete flow matching generative model with an efficient optimal transport for graph structures and it incorporates an edge-augmented graph transformer. Additionally, GGFlow introduces a novel goal-guided generation framework to control the generative trajectory of our model towards desired properties. GGFlow demonstrates superior performance on both unconditional and conditional generation tasks, outperforming existing baselines and underscoring its effectiveness and potential for wider application. Code: `https://github.com/Xiaoyang878/GGFlow`

1 Introduction

Graph structural data generation has become critically important across various domains, including social networks (Grover et al., 2019), drug design (Bilodeau et al., 2022), and neural architecture search (NAS) (Lee et al., 2020). Effective modeling of the intrinsic joint distribution and accurate description of topological structures of graphs are essential for these applications. Deep generative models have increasingly demonstrated success in graph generation by effectively modeling the complex structural properties of graphs. These models are typically categorized into autoregressive and one-shot types. Autoregressive models, such as GraphRNN

[*]Contributed equally: Author order is randomized and can be adjusted as needed for individual purposes.
[†]Correspondence should be addressed to Shiwei Sun (dwsun@ict.ac.cn) and Xin Gao (xin.gao@kaust.edu.sa)

(You et al., 2018), generate graphs sequentially, often overlooking the interdependencies among all graph components. In contrast, one-shot methods generate entire graphs in a single step, more effectively capturing the joint distribution (Ma et al., 2018; Luo et al., 2023; Niu et al., 2020).

Diffusion models have shown great promise and achieved significant performance in various domains (Ho et al., 2020; Song et al., 2020; Ho et al., 2022). In the context of graph generation, diffusion models have been adopted to enhance generative capacity. EDP-GNN and GDSS are among the first to utilize diffusion models for graph generation, adding continuous Gaussian noise to adjacency matrices and node types, which may lead to invalid graph structures (Niu et al., 2020; Jo et al., 2022b). Due to the inherent sparsity and discreteness of graph structures, GSDM enhances model fidelity by introducing Gaussian noise within a continuous spectrum space of the graph, DiGress and PPGN apply discrete diffusion models for graphs (Luo et al., 2023; Vignac et al., 2022; Austin et al., 2021; Haefeli et al., 2022; Huang et al., 2023).

Flow matching generative models also offer a compelling alternative. As these methods transform the training paradigm from SDEs to a more stable interpolation method, they enable more efficient sampling via ordinary differential equations (ODEs) (Lipman et al., 2022; Song et al., 2024; Yim et al., 2023). Furthermore, the application of optimal transport (OT) has been explored to straighten marginal probability paths, leading to reduced training variance and accelerated sampling (Bose et al., 2023; Tong et al., 2023; Klein et al., 2024; Pooladian et al., 2023). Nevertheless, the integration of OT into graph-based systems often encounters substantial computational hurdles due to the inherent complexity of computing OT metrics for discrete structures (Chen et al., 2020b; Petric Maretic et al., 2019).

In this paper, we introduce GGFlow, a novel generative model that leverages discrete flow matching techniques with an efficient optimal transport in graph generation. The model preserves graph sparsity and permutation invariance, which is essential for realistic graph generation. Additionally, GGFlow employs a goal-guided framework using reinforcement learning for conditional generation. GGFlow achieves state-of-the-art results in both unconditional and conditional graph and molecule generation tasks and surpasses existing methods. Its effectiveness in conditional generation tasks underscores the practical impact of our approach.

Our contribution can be summarized as:

- GGFlow introduces the first discrete flow matching generative model with an efficient optimal transport for graph data, and it also incorporates an edge-augmented graph transformer to enhance generation tasks further.
- GGFlow proposes a novel guidance framework using reinforcement learning to control probability flow during graph generation, targeting specific properties.
- GGFlow demonstrates state-of-the-art performance in various unconditional and conditional graph generation tasks, consistently outperforming existing methods across diverse graph types and complexities.

2 Related Work

2.1 Flow Matching and Diffusion Models

Diffusion models have gained widespread popularity in various fields, including computer vision, natural language processing, and biological sciences, demonstrating notable success in generative tasks (Ho et al., 2020; Song et al., 2020; Watson et al., 2023; Ingraham et al., 2023; Liu et al., 2024a; Ren et al., 2024; Zhu et al., 2024). Recently, flow matching generative models have emerged as a more efficient and stable alternative (details in Appendix A.1), improving generative performance (Lipman et al., 2022; Song et al., 2024; Campbell et al., 2024). Some approaches further enhance performance by incorporating optimal transport. The generative processes of these models are summarized in Figure 1.

Previous works (Campbell et al., 2024; Gat et al., 2024) extended flow matching to discrete spaces, while Eijkelboom et al. (2024) applied variational flow matching to graphs, but without adequately addressing key graph-specific properties such as adjacency matrix sparsity. GGFlow tackles these challenges by introducing

a discrete flow matching model with an efficient optimal transport tailored for graph data. Furthermore, we propose a novel framework for guiding the generative process, enhancing its practical applicability.

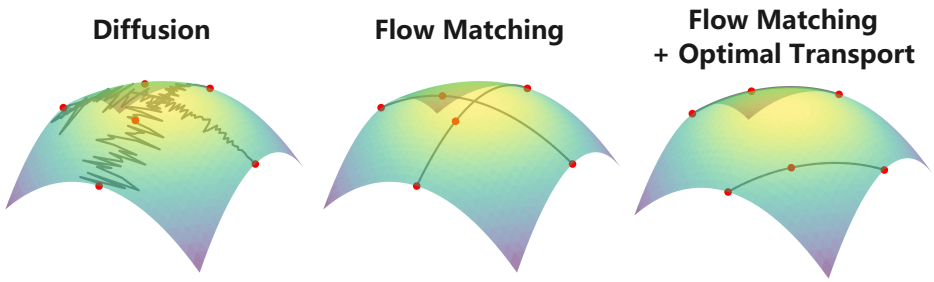

Figure 1: Illustration of generative trajectories using different methods. The generative trajectories are learned by the diffusion model (left), flow matching model (center), and flow matching model with optimal transport (right).

2.2 Graph Generative Models

Graph generative models are typically categorized into two main types: autoregressive and one-shot models. Autoregressive models generate graphs sequentially (Wang et al., 2018; You et al., 2018; Jin et al., 2018; Shi et al., 2019; Luo et al., 2021; Kong et al., 2023). While effective, these models are often computationally expensive and fail to account for permutation invariance, a crucial property for graph data, resulting in potential inefficiencies. In contrast, one-shot models aim to capture the distribution of all graph components simultaneously (De Cao & Kipf, 2018; Ma et al., 2018; Zang & Wang, 2020), better reflecting the inherent interactions within graphs. Despite the advantages, diffusion-based one-shot models (Niu et al., 2020; Jo et al., 2022b; Vignac et al., 2022; Chen et al., 2023; Bergmeister et al., 2023; Luo et al., 2023; Haefeli et al., 2022; Yan et al., 2023; Jang et al., 2023; Madeira et al., 2024; Bergmeister et al., 2024; Chen et al., 2023; Minello et al., 2024; Zhao et al., 2024; Xu et al., 2024) show promising results in downstream tasks. GGFlow employs a discrete flow-matching generative model, achieving superior generative performance. More comparisons with recent works are presented in Appendix B.

3 Methods

In this section, we present our methodology, GGFlow. Section 3.1 outlines the discrete flow matching method for graph generation. Section 3.2 covers an efficient optimal transport for graph flow matching. Section 3.3 introduces GraphEvo, our neural network for graph generation. Section 3.4 examines the permutation properties of GGFlow, and Section 3.5 discusses goal-guided graph generation using reinforcement learning.

3.1 Discrete Flow Matching for Graph Generation

A graph $G = (V, E)$, where V and E denote the sets of nodes and edges, has a distribution denoted by $p(G) = (p^V(V), p^E(E))$. The attribute spaces for nodes and edges are $\mathcal{V}$ and $\mathcal{E}$, with cardinalities n and m, respectively. The attributes of node i and edge ij are denoted by $v_i \in \mathcal{V}$ and $e_{ij} \in \mathcal{E}$, so the node and edge probability mass functions (PMF) are $p^V(v_i = a)$ and $p^E(e_{ij} = b)$ where $a \in \{1, \ldots, n\}$ and $b \in \{1, \ldots, m\}$. The node and edge encodings in the graph are given by matrices $\mathbf{V} \in \mathbb{R}^{a \times n}$ and $\mathbf{E} \in \mathbb{R}^{a \times a \times m}$, respectively. We denote the transpose of matrix $\mathbf{A}$ as $\mathbf{A}^*$ and $\mathbf{A}^t$ represents the state of matrix $\mathbf{A}$ at time t. We use discrete flow matching to model the graph generation process.

Source and target distribution GGFlow aims to transform prior distribution $G^0 \sim p_{\text{ref}}$ to target data distribution $G^1 \sim p_{\text{data}}$. The training data (G^0, G^1) are sampled from a joint distribution $\pi(G^0, G^1)$, satisfying the marginals constraints $p_{\text{ref}} = \sum_{G^1} \pi(G^0, G^1), p_{\text{data}} = \sum_{G^0} \pi(G^0, G^1)$. In the simplest case, the joint distribution $\pi(G^0, G^1)$ is modeled as the independent coupling, i.e. $\pi(G^0, G^1) = p_{\text{ref}} \cdot p_{\text{data}}$.

To account for graph sparsity, the prior distribution $p_{\text{ref}} = (p^V_{\text{ref}}, p^E_{\text{ref}})$ is designed to approximate the true data distribution closely. To ensure the permutation invariance of the model, the priors are structured as products of single distributions for all nodes and edges: $\prod_i v_i \times \prod_{ij} e_{ij}$ (Vignac et al., 2022). Further details on the prior can be found in Appendix C.1.

Probability path We define a probability path $p_t(G^t)$ that interpolates between source distribution p_{ref} and target distribution p_{data} i.e. $p_0 = p_{\text{ref}}$ and $p_1 = p_{\text{data}}$. The marginal probability path is given by:

$$p_t(G^t) = \sum_{(G^0,G^1)\sim\pi} p_t(G^t|G^0,G^1)\pi(G^0,G^1), \tag{1}$$

where

$$\begin{aligned} p_t(G^t|G^0,G^1) &= \text{Cat}\Big(t\delta\{G^1,G\} + (1-t)p_{\text{ref}}\Big) \\ &= \text{Cat}\Big(t\delta\{V^1,V\} + (1-t)p^V_{\text{ref}}, t\delta\{E^1,E\} + (1-t)p^E_{\text{ref}}\Big), \end{aligned}$$

δ is the Kronecker delta, indicating equality of the indices, and $\text{Cat}(p)$ denotes a Categorical distribution with probabilities p. Given the sparsity of both the prior and data distributions, we can infer that the intermediate distribution is similarly sparse, aiding model training.

We define a probability velocity field $u_t(G,G^t) = (u^V_t(V,V^t), u^E_t(E,E^t))$ for GGFlow, which generates the probability path from Equation 1. The probability velocity field $u_t(G,G^t)$ is derived from the conditional probability velocity field $u_t(G,G^t|G^0,G^1)$, and can be expressed as:

$$u_t(G,G^t) = \sum_{(G^0,G^1)} u_t(G,G^t|G^0,G^1)p_t(G^0,G^1|G), \tag{2}$$

$$p_t(G^0,G^1|G^t) = p_{1|t}(G^1|G^t,G^0)\frac{p_t(G^t|G^0,G^1)\pi(G^0,G^1)}{\sum_{G^0,G^1} p_t(G^t|G^0,G^1)\pi(G^0,G^1)}. \tag{3}$$

GGFlow chooses the conditional marginal probability $u_t(G,G^t|G^0,G^1)$ as:

$$u_t(G,G^t|G^0,G^1) = \frac{1}{\mathbf{Z}_t(1-t)p_{\text{ref}}}\delta\{G,G^1\}(1-\delta\{G^t,G^1\}), G^t \neq G, \tag{4}$$

where $\mathbf{Z}_t = |\{G^t : p_t(G^t|G^0,G^1) > 0\}|$. More details about the choice of the conditional vector field are provided in Appendix C.2.

Training objective Given the intractability of the posterior distribution $p_{1|t}(G^1|G^t,G^0)$, we approximate it as $\hat{p}_{1|t}(G^1|G^t,G^0)$ using neural network, as detailed in Section 3.3. The training objective is formulated as:

$$\mathcal{L} = \mathbb{E}_{p_{\text{data}}(G^1)\mathcal{U}(t;0,1)\pi(G^0,G^1)p_t(G^t|G^0,G^1)}[\log \hat{p}_{1|t}(G^1|G^t,G^0)], \tag{5}$$

where $\mathcal{U}(t;0,1)$ is a uniform distribution on $[0,1]$.

Sampling Procedure In the absence of the data distribution G^1 during sampling, we reparameterize the conditional probability $p_t(G^0,G^1|G^t)$ as:

$$\begin{aligned} p_t(G^0,G^1|G^t) &= p_{1|t}(G^1|G^t,G^0)\frac{p_t(G^t|G^0)p(G^0)}{\sum_{G^0} p_t(G^t|G^0)p(G^0)}. \\ p_t(G^t|G^0) &= \text{Cat}\Big(t\delta\{V^1,V\} + (1-t)p^{\text{ref}}_V, t\delta\{E^1,E\} + (1-t)p^{\text{ref}}_E\Big) \end{aligned}$$

And we can simplify the generative process $p_{t+\Delta t|t}(G^{t+\Delta t}|G^t,G^0)$ without the calculation of the full expectation over conditional vector field $u_t(G,G^t|G^0,G^1)$:

$$\begin{aligned} p_{t+\Delta t|t}(G^{t+\Delta t}|G^t,G^0) &= \mathbb{E}_{\hat{p}_t(G^1|G^t,G^0)}[\delta(G^t,G^{t+\Delta t}) + u_t(G^t,G^{t+\Delta t}|G^0,G^1)\Delta t] \\ &= \sum_{G^1} p_{t+\Delta t|t}(G^{t+\Delta t}|G^t,G^1,G^0)\hat{p}_{1|t}(G^1|G^t,G^0). \end{aligned} \tag{6}$$

We first sample the $\hat{G}^1$ using the approximate distribution $\hat{p}_{1|t}(G^1|G^t, G^0)$ and then sample the next state $G^{t+\Delta t}$ using sampled $\hat{G}^1$. The sampling procedure $p_{t+\Delta t|t}(G^{t+\Delta t}|G^1, G^t, G^0)$ can thus be formulated as:

$$G^{t+\Delta t} \sim \delta\{\cdot, G^t\} + u_t(\cdot, G^t|G^0, \hat{G}^1)\Delta t.$$

Further details on the sampling and training procedures are provided in Algorithms 1 and 4.

Algorithm 1 Sampling Procedure of GGFlow

Require: $t = 0, G^0 \sim (p_V^{\text{ref}}, p_E^{\text{ref}}), u_t(G, G^t|G^0, G^1), N_{\text{steps}}$
1: $\Delta t = 1/N_{\text{steps}}$
2: **for** $n \in \{0, \ldots, N_{\text{steps}} - 1\}$ **do**
3: $\quad \hat{p}_{1|t}(G^1|G^0, G^t) = \text{GraphEvo}(G^t, G^0, t)$
4: $\quad \hat{G}^1 \sim \hat{p}_{1|t}(\cdot|G^0, G^t)$
5: $\quad$ // Sampling from the conditional velocity field
6: $\quad G^{t+\Delta t} \sim \delta\{\cdot, G^t\} + u_t(\cdot, G^t|G^0, \hat{G}^1)\Delta t$
7: $\quad t = t + \Delta t$
8: **end for**
9: **return** $G^1 = (V^1, E^1)$

3.2 Efficient Optimal transport for graph flow matching

Optimal transport (OT) has been effectively applied to flow matching generative models in continuous variable spaces, to improve generative performance (Tong et al., 2023; Bose et al., 2023; Song et al., 2024). To generalize this for graphs, we extend the joint distribution $\pi(G^0, G^1)$ from independent coupling to the 2-Wasserstein OT map ϕ^*, which minimizes the 2-Wasserstein distance between p_{ref} and p_{data}. To optimize the computational efficiency of OT, we define the distance via the Hamming distance $H(G^0, G^1)$ (Bookstein et al., 2002):

$$\phi^*(p_0, p_1) = \arg\inf_{\phi \in \Phi} \int_{\mathbb{R}^d \times \mathbb{R}^d} H(G^0, G^1) \mathrm{d}\phi(G^0, G^1), \tag{7}$$

where

$$H(G^0, G^1) = \sum_i \delta(v_i^0, v_i^1) + \lambda \sum_{i,j} \delta(e_{ij}^0, e_{ij}^1). \tag{8}$$

Here Φ represents the set of all joint probability measures on $\mathbb{R}^d \times \mathbb{R}^d$ that are consistent with the marginal distributions p_0 and p_1, where $G^K = (V^K = \{v_i^K\}, E^K = \{e_{ij}^K\}_{ij})$, $K = 0, 1$.

The practical application of OT to large datasets is computationally intensive, often requiring cubic time complexity and quadratic memory (Tong et al., 2020; Villani, 2009). To address these challenges, we use a minibatch approximation of OT (Fatras et al., 2021). A detailed analysis of optimal transport during the training procedure is provided in Appendix E.

3.3 GraphEvo: Edge-augmented Graph Transformer

Our neural network, GraphEvo, predicts the posterior distribution $\hat{p}_{1|t}(G^1|G^t, G^0)$ using the intermediate graph G^t and initial noise graph G^0. In graph-structured data, edge and structural information are as critical as node attributes, and incorporating edge relations enhances link generation tasks (Hussain et al., 2024; Hou et al., 2024; Jumper et al., 2021). To capture these relations, GraphEvo extends the graph transformer by introducing a triangle attention mechanism for edge updates, along with additional graph features y, such as cycles and the number of connected components (Vignac et al., 2022). This enables GraphEvo to efficiently and accurately capture the joint distribution of all graph components. The key self-attention mechanisms are outlined in Algorithm 2, where node, edge, and graph features are represented as $\mathbf{X} \in \mathbb{R}^{bs \times n \times dx}$, $\mathbf{E} \in \mathbb{R}^{bs \times n \times dx}$, and $\mathbf{y} \in \mathbb{R}^{bs \times n \times dy}$, where bs denotes batch size, n is the number of nodes, and dx and dy are the feature dimensions for node and global features, respectively. Further details are provided in Appendix D.

Algorithm 2 Self-attention Mechanism in GraphEvo

Require: $\mathbf{X} \in \mathbb{R}^{bs \times n \times dx}, \mathbf{E} \in \mathbb{R}^{bs \times n \times dx}, \mathbf{y} \in \mathbb{R}^{bs \times n \times dy}$

$\mathbf{Q}, \mathbf{K}, \mathbf{V} \leftarrow \text{Linear}(\mathbf{X})$

$\mathbf{Y} \leftarrow \frac{\mathbf{Q} \times \mathbf{K}}{\sqrt{d_{\mathbf{Y}}}}$ // Calculation attention score for node embedding

$\mathbf{Y} \leftarrow \text{FiLM}(\mathbf{Y}, \mathbf{E})$ // Incorporate edge features to self-attention scores

$\mathbf{E} \leftarrow \mathbf{Y}$

$\mathbf{Q_e}, \mathbf{K_e}, \mathbf{V_e}, \mathbf{b}, \mathbf{g} \leftarrow \text{Linear}(\mathbf{E})$

$\mathbf{Y_e} \leftarrow \frac{\mathbf{Q_e} \times \mathbf{K_e}}{\sqrt{d_{\mathbf{Y_e}}}} + \mathbf{b}$ // Calculation triangle attention score for edge embedding

$\mathbf{E} \leftarrow \mathbf{Y_e} * \mathbf{V_e} * \text{sigmoid}(\mathbf{g})$

$\mathbf{E} \leftarrow \text{Linear}\Big(\text{FiLM}(\mathbf{E}, \mathbf{y})\Big)$ // Incorporate global structural features to edge embedding

$\mathbf{X} \leftarrow \mathbf{Y} * \mathbf{V}$

$\mathbf{X} \leftarrow \text{Linear}\Big(\text{FiLM}(\mathbf{X}, \mathbf{y})\Big)$ // Incorporate global structural features to node embedding

$\mathbf{y} \leftarrow \text{Linear}\Big(\text{Linear}(\mathbf{y}) + \text{PNA}(\mathbf{X}) + \text{PNA}(\mathbf{E})\Big)$

return $\mathbf{X}, \mathbf{E}, \mathbf{y}$

3.4 Permutation Property Analysis

Graphs are invariant to random node permutations, and GGFlow preserves this property. To ensure permutation invariance, we analyze the permutation properties of our neural network, training objectives, and conditional probabilities path. First, we analyze the permutation invariance of the training objectives (Vignac et al., 2022). Since the source and target distributions are permutation invariant, the independent coupling also exhibits this invariance. Our optimal transport map, derived from Equation 7, similarly demonstrates invariance to identical permutations. Further clarifications regarding optimal transport can be found in Appendix C.4.

Theorem 1. *If the distributions $p(G^0)$ and $p(G^1)$ are permutation invariant, and the cost function maintains invariance under identical permutations, i.e., $H(G^0, G^1) = H(\pi G^0, \pi G^1)$ for any permutation π, then the optimal transport map ϕ also exhibits invariance under identical permutations, such that $\phi(G^0, G^1) = \phi(\pi G^0, \pi G^1)$.*

Proof of this theorem can be found in Appendix C.4. To ensure that the generated graph retains its identity under random permutations, the generated distribution must remain exchangeable, and GraphEvo must be permutation equivariant.

Proposition 1. *The distribution generated by the conditional flow is exchangeable with respect to nodes and graphs, i.e. $p(\mathbf{V}, \mathbf{E}) = \mathbf{p}(\pi^* \mathbf{V}, \pi^* \mathbf{E} \pi)$, where π is a permutation operator.*

Proposition 2. *GraphEvo is permutation equivariant.*

The proofs of Proposition 1 and 2 are provided in Appendix C.3 and Appendix D.1, respectively.

3.5 Goal-Guided Framework for Conditional Generation

For practical applications such as drug discovery, we propose a goal-guided framework for discrete flow matching, employing reinforcement learning (RL) to guide graph flow matching models for non-differentiable objectives. The goal of the guidance method is to map the noise distribution p_0 to a preference data distribution p_1^* using a reward function $\mathcal{R}(G^t, t)$.

We formulate the inference process of flow matching as a Markov Decision Process (MDP), where (G^t, t) and $G^{t+\Delta t}$ are the state space $\mathbf{s}_t$ and action space $\mathbf{a}_t$, p_0 is an initial noise distribution, $p_{t+\Delta t|t}(G^{t+\Delta t}|G^t, t)$ is the transition dynamics and policy network $\pi(\mathbf{a}_t|\mathbf{s}_t)$, $\mathcal{R}(G^t, t) = r(G^1)\mathbb{I}[t = 1]$ is the reward function

To enable exploration, we introduce a temperature parameter T for the policy network during sampling, allowing the model to explore a broader space at higher temperatures:

$$\pi(\mathbf{a}_t|\mathbf{s}_t) = p_{t+\Delta t|t}(G^{t+\Delta t}|G^t, t) = \mathrm{Cat}\Big((\delta\{\cdot, G^t\} + u_t(\cdot, G^t|G^0, \hat{G}^1)\Delta t)/T\Big) \tag{9}$$

The goal of RL training is to maximize the reward function. To prevent overfitting to the reward preference distribution, we add a Kullback–Leibler (KL) divergence term between the Reinforcement learning fine-tuned model $p_\theta^{RL}(\cdot)$ and pre-trained model $p_\theta(\cdot)$ (Ouyang et al., 2022).

We employ the policy gradient method to update the network, where the policy is refined to $\pi(\mathbf{a}_t|\mathbf{s}_t) = p_\theta^{(T)}(G^1|G^t)q(G^{t+\Delta t}|G^1)$ to $\pi(\mathbf{a}_t|\mathbf{s}_t) = p_\theta^{(T)}(G^1|G^t)$ (Sutton et al., 1999; Liu et al., 2024b), directly increasing the probability of generating G^1 with higher rewards at all timestep t. The training objective is:

$$\mathcal{L}_{RL} = -\mathbb{E}_{p_\theta(G^{0:t:1})}[\alpha\mathcal{R}(G^1)\sum_{t=0}^{t=1}\log p_\theta^{RL}(G^1|G^t, G^0) - \beta\sum_{t=0}^{t=1}\mathrm{KL}(p_\theta^{RL}(G^1|G^t, G^0)||p_\theta(G^1|G^t, G^0))] \tag{10}$$

where $p_\theta(G^{0:t:1})$ represents $p_{\mathrm{data}}(G^1)\mathcal{U}(t; 0, 1)\pi(G^0, G^1)p_t(G^t|G^0, G^1)$. Using this optimization objective, we fine-tune the pre-trained flow matching model to generate data following the preference distribution. By integrating optimal transport, we optimize the pairing of prior data and high-reward training data (Chen et al., 2020a). The pseudo-code for the guided GGFlow training is provided in Algorithm 5 and a toy example is shown in Appendix F.

4 Experiments

To validate the performance of our method, we compare GGFlow with state-of-the-art graph generative baselines on generic graph generation and molecule generation, over several benchmarks in Section 4.1 and Section 4.2, respectively. The ability of GGFlow to perform conditional generation is analyzed in Section 4.3. Finally, we conduct detailed ablation studies presented in Section 4.4.

4.1 Generic Graph Generation

We evaluated GGFlow on five generic graph generation benchmarks of varying sizes: Ego-small, Community-small, Grid, Planar and Enzymes. We employ the same train/test split as GraphRNN (You et al., 2018), utilizing 80% of each dataset for training and the remaining for testing. We compared GGFlow's performance against well-known autoregressive models: DeepGMG (Li et al., 2018), GraphRNN (You et al., 2018), GraphAF (Shi et al., 2019), and GraphDF (Luo et al., 2021) and one-shot models: GraphVAE (Simonovsky & Komodakis, 2018), GNF (Liu et al., 2019), EDP-GNN (Niu et al., 2020), GDSS (Jo et al., 2022a), DiGress (Vignac et al., 2022), GRASP (Minello et al., 2024), GSDM (Luo et al., 2023), GruM (Jo et al., 2024), and SwinGNN (Yan et al., 2023). Consistent with previous studies, we generated an equal number of graphs as the test set to compare distributions of graph statistics, including degree distribution (Deg.), clustering coefficient (Clus.), and the frequency of 4 node orbits (Orbit). Detailed descriptions of datasets, baselines, and metrics are provided in Appendix H.

Table 1 presents our results, showing that GGFlow achieves superior performance across most metrics. Additionally, GGFlow demonstrates comparable performance compared to state-of-the-art models in generating large graphs on the Grid dataset. These findings underscore the effectiveness of GGFlow at capturing the local characteristics and data distributions of graphs. Additional metrics and dataset experimental results are included in Appendix G, and we visualize the generated graphs in Appendix J.

4.2 Molecule Graph Generation

We evaluated GGFlow on two standard molecular datasets, QM9 (Ramakrishnan et al., 2014) and ZINC250k (Irwin et al., 2012), using several metrics: Validity, Validity without correction, Neighborhood Subgraph Pairwise Distance Kernel (NSPDK) Maximum Mean Discrepancy (MMD), and Frechet ChemNet Distance (FCD). To calculate these metrics, we sampled 10,000 molecules. We compared GGFlow against various

Table 1: Generation results on the generic graph datasets. Results are the means of 3 different runs. The best results and the second-best results are marked **bold** and bold.

Method	Ego-small				Community-small				Grid				Step
	Deg.	Clus.	Orbit	Avg.	Deg.	Clus.	Orbit	Avg.	Deg.	Clus.	Orbit	Avg.	
Training Set	0.014	0.022	0.004	0.013	0.003	0.009	0.001	0.005	0.000	0.000	0.000	0.000	-
DeepGMG	0.040	0.100	0.020	0.053	0.220	0.950	0.400	0.523	-	-	-	-	-
GraphRNN	0.090	0.220	0.003	0.104	0.080	0.120	0.040	0.080	0.064	0.043	0.021	0.043	-
GraphAF	0.031	0.107	**0.001**	0.046	0.178	0.204	0.022	0.135	-	-	-	-	-
GraphDF	0.039	0.128	0.012	0.046	0.060	0.116	0.030	0.069	-	-	-	-	-
GNF	0.030	0.100	**0.001**	0.044	0.200	0.200	0.110	0.170	-	-	-	-	-
GraphVAE	0.137	0.166	0.051	0.118	0.358	0.969	0.551	0.626	1.594	**0.000**	0.904	0.833	-
EDP-GNN	0.054	0.092	0.007	0.051	0.050	0.159	0.027	0.079	0.460	0.243	0.316	0.340	1000
GDSS	0.027	**0.033**	0.008	0.022	0.044	0.098	0.009	0.058	0.133	0.009	0.123	0.088	1000
GSDM	-	-	-	-	0.020	0.050	0.005	0.053	0.002	**0.000**	**0.000**	0.001	1000
DiGress	0.028	0.046	0.008	0.027	0.032	0.047	0.009	0.025	0.037	0.046	0.069	0.051	500
SwinGNN	0.017	0.060	0.003	0.027	**0.006**	0.125	0.018	0.050	**0.000**	**0.000**	**0.000**	**0.000**	500
GGFlow	**0.005**	**0.033**	0.004	**0.014**	0.011	**0.030**	**0.002**	**0.014**	0.030	**0.000**	0.016	0.015	500

molecule generation models, including GraphAF, GraphDF, MolFlow (Zang & Wang, 2020), EDP-GNN, GraphEBM (Liu et al., 2021), GDSS, PS-VAE (Kong et al., 2022), MolHF (Zhu et al., 2023), GruM, SwinGNN, DiGress, and GSDM. Detailed descriptions of the datasets, baselines and metrics are provided in Appendix H.

The results, presented in Table 2, indicate that GGFlow effectively captures the distribution of molecular data, showing significant improvements over the baselines. The high Validity without correction suggests that GGFlow successfully learns chemical valency rules. Additionally, GGFlow achieves superior NSPDK and FCD scores on both datasets, demonstrating its ability to generate molecules with distributions closely resembling those of natural molecules. Visualizations of molecules generated by different models are shown in Figure 2, with additional results on GGFlow provided in Appendix J.

Table 2: Generation results on the QM9 and ZINC250k datasets. Results are the means of 3 different runs. The best results and the second-best results are marked **bold** and bold.

Method	QM9				ZINC250k				Step
	Val.	Val. w/o corr.	NSPDK	FCD	Val.	Val. w/o corr.	NSPDK	FCD	
Training Set	100	100	0.0001	0.040	100	100	0.0001	0.062	-
GraphAF	100	67.14	0.0218	5.246	100	67.92	0.0432	16.128	-
GraphDF	100	83.14	0.0647	10.451	100	89.72	0.1737	33.899	-
MolFlow	100	92.03	0.0169	4.536	100	63.76	0.0468	20.875	-
GraphEBM	100	8.78	0.0287	6.402	100	5.29	0.2089	35.467	-
PS-VAE	-	-	0.0077	1.259	-	-	0.0112	6.320	-
MolHF	-	-	-	-	100	93.62	0.0387	23.940	-
EDP-GNN	100	47.69	0.0052	2.683	100	83.16	0.0483	16.819	1000
GDSS	100	96.17	0.0033	2.565	100	97.12	0.0192	14.032	1000
GSDM	100	99.90	0.0034	2.614	100	92.57	0.0168	12.435	1000
GruM	100	99.69	**0.0002**	0.108	100	98.32	0.0023	2.235	1000
SwinGNN	100	99.66	0.0003	0.118	100	86.16	0.0047	4.398	500
DiGress	100	98.29	0.0003	**0.095**	100	94.98	0.0021	3.482	500
GGFlow	100	**99.91**	**0.0002**	0.148	100	**99.63**	**0.0010**	**1.455**	500

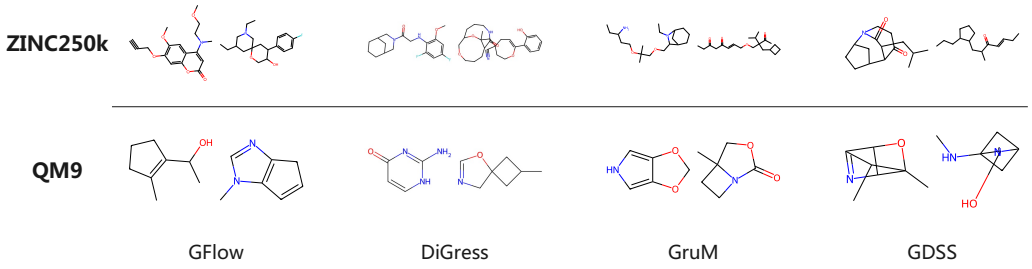

Figure 2: Visualization of generated samples of different models in different molecular datasets

4.3 Conditional Generation

To further evaluate the performance of our model, we conducted conditional generation experiments on the QM9 dataset, focusing on generating molecules with molecular properties μ that closely match a target value μ^*. In the experiment, we set the target value as 1, i.e. $\mu^* = 1$.

For the experiment, we employed a reinforcement learning-based guidance method and compared it to the guided version of DiGress, which also proposes an effective approach for discrete diffusion models in conditional generation tasks. The reward function was defined as $|\mu - \mu^*|$, and the model was trained over 10,000 steps using the training settings detailed in Section 4.2. To evaluate the effectiveness of our guidance method, we compared it against three baselines: (1) Guidance for DiGress (Vignac et al., 2022). (2) Direct supervised training (ST) (3) Supervised fine-tuning (SFT). Additionally, we calculated the mean and variance of $|\mu - \mu^*|$for samples generated unconditionally by both DiGress and GGFlow to provide a baseline comparison. Further details of the experiment are provided in Appendix H.5.

The results, detailed in Table 3, demonstrate the superiority of our reinforcement learning-based conditional generation method over both ST and SFT approaches. Notably, our method surpasses the guidance techniques used in diffusion models, showcasing its enhanced ability to steer the generative process toward desired outcomes. Additionally, our approach achieves higher validity in conditional generated tasks, highlighting its robustness and superior performance in goal-directed generation.

Table 3: Mean absolute error of molecular property μ on conditional generation on the QM9 dataset.

Methods	DiGress		GGFlow			
	Uncondition	+Guidance	Unconditition	Supervised Training	+SFT	+RL
Mean	1.562	1.092	1.569	1.184	1.223	**0.672**
Variance	1.641	0.894	1.987	1.579	1.893	**0.647**
Val. w/o corr.	96.54	74.2	98.93	86.1	87.0	**92.2**

4.4 Ablation studies

To thoroughly assess the individual contributions of the proposed components to GGFlow's performance, we conducted a comprehensive series of ablation experiments. These studies utilized both the Community-small and ZINC250k datasets. Our investigation focused on isolating the impact of: (1) the full GGFlow model, (2) the model performance without the integration of Optimal Transport (OT), denoted as GGFlow (w/o OT), (3) the model performance without the GraphEvo module, denoted as GGFlow (w/o Evo), and (4) the baseline GGFlow framework without either the GraphEvo module or Optimal Transport, designated as GGFlow (w/o both). The specific configurations for each ablated model are summarized in Table 4. The empirical results of these studies are presented in detail in Table 5. Further specifics regarding the experimental setup are provided in Appendix I.2.

Table 4: Ablated model configurations used in the study.

Method	Flow Matching Framework	Optimal Transport	GraphEvo Module
DiGress	✗	✗	✗
GGFlow (w/o both)	✓	✗	✗
GGFlow (w/o OT)	✓	✗	✓
GGFlow (w/o Evo)	✓	✓	✗
GGFlow	✓	✓	✓

As demonstrated in Table 5, a comparative analysis of GGFlow (w/o OT) and GGFlow reveals that the integration of Optimal Transport consistently improves generation performance. Notably, even in the absence of both GraphEvo and Optimal Transport, GGFlow (w/o both) consistently outperforms DiGress, thereby underscoring the inherent advantages of our flow matching framework over traditional diffusion models in graph generation tasks.

Furthermore, the GraphEvo module, particularly its triangle attention mechanism for edges, effectively captures more intricate node and edge features, leading to substantial performance enhancements. To investigate GraphEvo's ability to extract edge information, we calculated the cross-entropy of edges on the validation set for each epoch in Figure S4. We observed that after incorporating GraphEvo, the edge cross-entropy decreased more rapidly, indicating the model's enhanced capability in capturing edge information.

Table 5: Ablation studies on the OT and GraphEvo on the Commuinty-small and ZINC250k datasets. Results are the means of 3 different runs. The best results are marked **bold**.

Method	**Community-small**			**ZINC250k**			**Step**
	Deg.	Clus.	Orbit	Val. w/o corr.	NSPDK	FCD	
DiGress	0.032	0.047	0.009	94.98	0.0021	3.482	500
GGFlow (w/o both)	0.028	0.076	0.007	99.07	0.0022	2.104	500
GGFlow (w/o OT)	0.018	**0.027**	0.004	99.58	0.0015	1.503	500
GGFlow (w/o Evo)	0.015	0.055	0.005	99.12	0.0025	1.891	500
GGFlow	**0.011**	0.030	**0.002**	**99.63**	**0.0010**	**1.455**	500

To evaluate the benefits of Optimal Transport on sampling efficiency, we conducted experiments with varying inference steps, as presented in Figure 3 (More detailed comparison on Community-small datasets in Figure S3). Our findings indicate that GGFlow achieves superior performance compared to other diffusion-based models with significantly fewer inference steps, particularly at 100 and 200 steps. This highlights GGFlow's enhanced sampling efficiency. Furthermore, the integration of Optimal Transport demonstrably boosts sampling efficiency and enhances generative performance across both generic and molecular graph generation tasks, as evidenced by the performance gains observed.

To demonstrate the enhanced training stability conferred by Optimal Transport and the Flow Matching framework, we performed a detailed analysis of evaluation metrics during the training phase. We compared the average values on the Community-small dataset and FCD values on the ZINC250k dataset against DiGress, which shares similar training objectives. For a fair comparison and to highlight the distinct contributions, we specifically focused on GGFlow (w/o both) and GGFlow (w/o Evo). Test set average values and FCD were computed as described in Section 4.1, utilizing checkpoints saved every 100 training steps.

To quantitatively assess training stability, we calculated the Mean Absolute Difference (MAD) of evaluation metric values between adjacent epochs and averaged these differences. As depicted in Figure 4, the presence

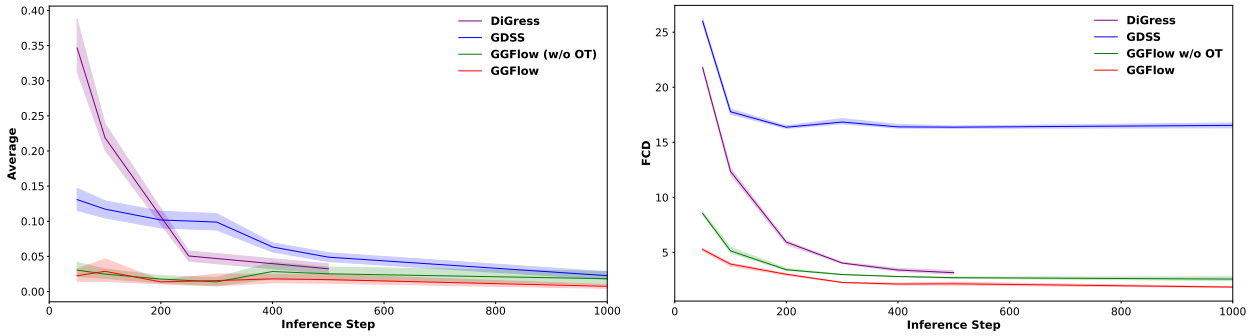

(a) Community-small (b) ZINC250k

Figure 3: Ablation studies on the impact of varying inference steps across Community-small and ZINC250k datasets. Performance of the ZINC250k dataset is evaluated using 1,000 generated molecules due to the computational cost of generating larger sets for metric calculation.

of Optimal Transport (comparing GGFlow (w/o Evo) to GGFlow (w/o both)) improved model stability, leading to more consistent performance during training.

Figure 4 further illustrates that both GGFlow (w/o both) and GGFlow (w/o Evo) achieve faster and more effective convergence than DiGress. Importantly, GGFlow (w/o Evo) consistently outperforms GGFlow (w/o both) in terms of both average metrics and FCD, clearly demonstrating the benefits derived from Optimal Transport. These findings collectively indicate that both the Optimal Transport module and the underlying Flow Matching framework significantly contribute to greater training stability.

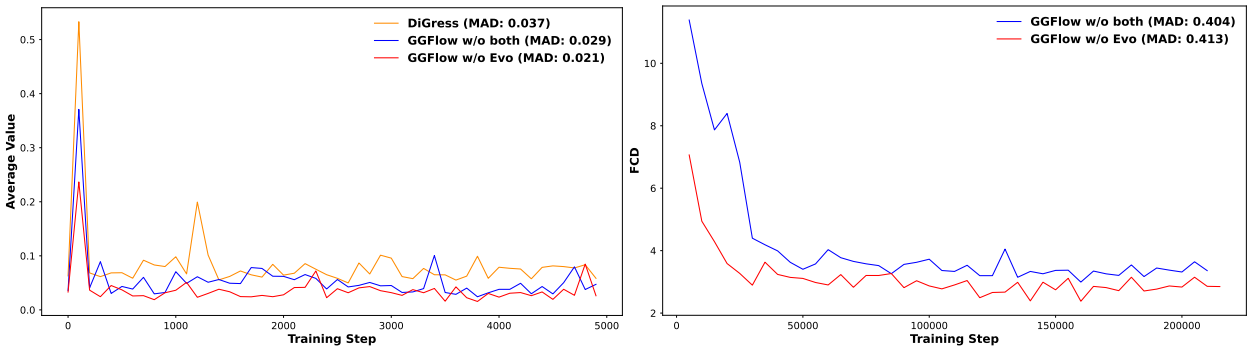

(a) Community-small (b) ZINC250k

Figure 4: Analysis of training stability for the Flow Matching framework and Optimal Transport on the Community-small and ZINC250k datasets. Test metrics of ZINC250k are calculated using 1,000 generated molecules.

5 Conclusion

In this paper, we introduced GGFlow, a discrete flow matching generative model for graphs that incorporates optimal transport and an innovative graph transformer network. GGFlow achieves state-of-the-art performance in unconditional graph generation tasks. Additionally, we presented a novel guidance method using reinforcement learning to control the generative trajectory toward a preferred distribution. Furthermore, our model demonstrates the ability to achieve the best performance across various tasks compared to other baselines, which highlights the practical impact of our guidance method. Despite these advancements, GGFlow has a primary limitation in its scalability to large graphs (with more than 500 nodes). This is primarily due to the computational complexity of the triangle attention updates and spectral feature computations. Generation times for different graph scales are provided in Appendix I.3. Another area for future work

is to improve the theoretical guarantees of our optimal transport method, as its current formulation only provides invariance to identical permutations rather than full permutation equivariance. Future research will focus on enhancing the scalability of GGFlow to larger graphs. We will also explore more generalized and efficient optimal transport methods that are fully permutation-invariant to strengthen the model's theoretical foundation and broaden its applicability.

6 Acknowledgments

This work was supported by the National Natural Science Foundation of China under Grants No. 82130055, 32271297, and 32370657; the National Key Research and Development Program of China under Grant No. 2020YFA0907000; the Key Special Project for Technological Innovation and Application Development of Chongqing Municipality under Grant No. CSTB2022TIAD-DEX0035; the King Abdullah University of Science and Technology (KAUST) Office of Research Administration (ORA) under Awards No. REI/1/5289-01-01, REI/1/5992-01-01, URF/1/6713-01-01, and FCC/1/5932-12-11; Center of Excellence for Smart Health (KCSH) under award number 5932; and Center of Excellence on Generative AI under award number 5940. The data underlying this article are available from the first and corresponding author upon reasonable request.

References

Jacob Austin, Daniel D Johnson, Jonathan Ho, Daniel Tarlow, and Rianne Van Den Berg. Structured Denoising Diffusion Models in Discrete State-Spaces. *Advances in Neural Information Processing Systems*, 34:17981–17993, 2021.

Andreas Bergmeister, Karolis Martinkus, Nathanaël Perraudin, and Roger Wattenhofer. Efficient and Scalable Graph Generation through Iterative Local Expansion. *arXiv preprint arXiv:2312.11529*, 2023.

Andreas Bergmeister, Karolis Martinkus, Nathanaël Perraudin, and Roger Wattenhofer. Efficient and scalable graph generation through iterative local expansion. In *The Twelfth International Conference on Learning Representations*, 2024.

Camille Bilodeau, Wengong Jin, Tommi Jaakkola, Regina Barzilay, and Klavs F Jensen. Generative models for molecular discovery: Recent advances and challenges. *Wiley Interdisciplinary Reviews: Computational Molecular Science*, 12(5):e1608, 2022.

Abraham Bookstein, Vladimir A Kulyukin, and Timo Raita. Generalized Hamming Distance. *Information Retrieval*, 5:353–375, 2002.

Joey Bose, Tara Akhound-Sadegh, Kilian FATRAS, Guillaume Huguet, Jarrid Rector-Brooks, Cheng-Hao Liu, Andrei Cristian Nica, Maksym Korablyov, Michael M Bronstein, and Alexander Tong. SE (3)-Stochastic Flow Matching for Protein Backbone Generation. In *The Twelfth International Conference on Learning Representations*, 2023.

Andrew Campbell, Joe Benton, Valentin De Bortoli, Thomas Rainforth, George Deligiannidis, and Arnaud Doucet. A Continuous Time Framework for Discrete Denoising Models. *Advances in Neural Information Processing Systems*, 35:28266–28279, 2022.

Andrew Campbell, Jason Yim, Regina Barzilay, Tom Rainforth, and Tommi Jaakkola. Generative Flows on Discrete State-Spaces: Enabling Multimodal Flows with Applications to Protein Co-Design. *arXiv preprint arXiv:2402.04997*, 2024.

Liqun Chen, Ke Bai, Chenyang Tao, Yizhe Zhang, Guoyin Wang, Wenlin Wang, Ricardo Henao, and Lawrence Carin. Sequence generation with optimal-transport-enhanced reinforcement learning. In *Proceedings of the AAAI Conference on Artificial Intelligence*, volume 34, pp. 7512–7520, 2020a.

Liqun Chen, Zhe Gan, Yu Cheng, Linjie Li, Lawrence Carin, and Jingjing Liu. Graph optimal transport for cross-domain alignment. In *International Conference on Machine Learning*, pp. 1542–1553. PMLR, 2020b.

Xiaohui Chen, Jiaxing He, Xu Han, and Li-Ping Liu. Efficient and Degree-Guided Graph Generation via Discrete Diffusion Modeling. In *Proceedings of the 40th International Conference on Machine Learning*, pp. 4585–4610, 2023.

Nicola De Cao and Thomas Kipf. MolGAN: An implicit generative model for small molecular graphs. *ICML 2018 workshop on Theoretical Foundations and Applications of Deep Generative Models*, 2018.

Floor Eijkelboom, Grigory Bartosh, Christian Andersson Naesseth, Max Welling, and Jan-Willem van de Meent. Variational flow matching for graph generation. *arXiv preprint arXiv:2406.04843*, 2024.

Paul Erdős, Alfréd Rényi, et al. On the evolution of random graphs. *Publ. math. inst. hung. acad. sci*, 5(1): 17–60, 1960.

Kilian Fatras, Younes Zine, Szymon Majewski, Rémi Flamary, Rémi Gribonval, and Nicolas Courty. Minibatch optimal transport distances; analysis and applications. *arXiv preprint arXiv:2101.01792*, 2021.

Itai Gat, Tal Remez, Neta Shaul, Felix Kreuk, Ricky TQ Chen, Gabriel Synnaeve, Yossi Adi, and Yaron Lipman. Discrete flow matching. *arXiv preprint arXiv:2407.15595*, 2024.

Aditya Grover, Aaron Zweig, and Stefano Ermon. Graphite: Iterative Generative Modeling of Graphs. In *International conference on machine learning*, pp. 2434–2444. PMLR, 2019.

Kilian Konstantin Haefeli, Karolis Martinkus, Nathanaël Perraudin, and Roger Wattenhofer. Diffusion models for graphs benefit from discrete state spaces. In *NeurIPS 2022 Workshop: New Frontiers in Graph Learning*, 2022.

Jonathan Ho, Ajay Jain, and Pieter Abbeel. Denoising Diffusion Probabilistic Models. *Advances in neural information processing systems*, 33:6840–6851, 2020.

Jonathan Ho, Tim Salimans, Alexey Gritsenko, William Chan, Mohammad Norouzi, and David J Fleet. Video Diffusion Models. *Advances in Neural Information Processing Systems*, 35:8633–8646, 2022.

Xiaoyang Hou, Tian Zhu, Milong Ren, Bo Duan, Chunming Zhang, Dongbo Bu, and Shiwei Sun. Gtam: A molecular pretraining model with geometric triangle awareness. *Bioinformatics*, pp. btae524, 2024.

Han Huang, Leilei Sun, Bowen Du, and Weifeng Lv. Conditional diffusion based on discrete graph structures for molecular graph generation. In *Proceedings of the AAAI Conference on Artificial Intelligence*, volume 37, pp. 4302–4311, 2023.

Md Shamim Hussain, Mohammed J Zaki, and Dharmashankar Subramanian. Triplet interaction improves graph transformers: Accurate molecular graph learning with triplet graph transformers. In *Forty-first International Conference on Machine Learning*, 2024. URL `https://openreview.net/forum?id=iPFuWc1TV2`.

John B Ingraham, Max Baranov, Zak Costello, Karl W Barber, Wujie Wang, Ahmed Ismail, Vincent Frappier, Dana M Lord, Christopher Ng-Thow-Hing, Erik R Van Vlack, et al. Illuminating protein space with a programmable generative model. *Nature*, pp. 1–9, 2023.

John J Irwin, Teague Sterling, Michael M Mysinger, Erin S Bolstad, and Ryan G Coleman. ZINC: A Free Tool to Discover Chemistry for Biology. *Journal of chemical information and modeling*, 52(7):1757–1768, 2012.

Yunhui Jang, Seul Lee, and Sungsoo Ahn. A Simple and Scalable Representation for Graph Generation. In *The Twelfth International Conference on Learning Representations*, 2023.

Wengong Jin, Regina Barzilay, and Tommi Jaakkola. Junction Tree Variational Autoencoder for Molecular Graph Generation. In *International conference on machine learning*, pp. 2323–2332. PMLR, 2018.

Jaehyeong Jo, Seul Lee, and Sung Ju Hwang. Score-based Generative Modeling of Graphs via the System of Stochastic Differential Equations. *arXiv:2202.02514*, 2022a. URL `https://arxiv.org/abs/2202.02514`.

Jaehyeong Jo, Seul Lee, and Sung Ju Hwang. Score-based Generative Modeling of Graphs via the System of Stochastic Differential Equations. In *International Conference on Machine Learning*, pp. 10362–10383. PMLR, 2022b.

Jaehyeong Jo, Dongki Kim, and Sung Ju Hwang. Graph generation with diffusion mixture. In *Forty-first International Conference on Machine Learning*, 2024.

John Jumper, Richard Evans, Alexander Pritzel, Tim Green, Michael Figurnov, Olaf Ronneberger, Kathryn Tunyasuvunakool, Russ Bates, Augustin Žídek, Anna Potapenko, et al. Highly accurate protein structure prediction with AlphaFold. *Nature*, 596(7873):583–589, 2021.

Leon Klein, Andreas Krämer, and Frank Noé. Equivariant flow matching. *Advances in Neural Information Processing Systems*, 36, 2024.

Lingkai Kong, Jiaming Cui, Haotian Sun, Yuchen Zhuang, B Aditya Prakash, and Chao Zhang. Autoregressive diffusion model for graph generation. In *International conference on machine learning*, pp. 17391–17408. PMLR, 2023.

Xiangzhe Kong, Wenbing Huang, Zhixing Tan, and Yang Liu. Molecule generation by principal subgraph mining and assembling. *Advances in Neural Information Processing Systems*, 35:2550–2563, 2022.

Hayeon Lee, Eunyoung Hyung, and Sung Ju Hwang. Rapid Neural Architecture Search by Learning to Generate Graphs from Datasets. In *International Conference on Learning Representations*, 2020.

Yujia Li, Oriol Vinyals, Chris Dyer, Razvan Pascanu, and Peter Battaglia. Learning Deep Generative Models of Graphs. *arXiv preprint arXiv:1803.03324*, 2018.

Yaron Lipman, Ricky TQ Chen, Heli Ben-Hamu, Maximilian Nickel, and Matthew Le. Flow Matching for Generative Modeling. In *The Eleventh International Conference on Learning Representations*, 2022.

Jenny Liu, Aviral Kumar, Jimmy Ba, Jamie Kiros, and Kevin Swersky. Graph Normalizing Flows. *Advances in Neural Information Processing Systems*, 32, 2019.

Meng Liu, Keqiang Yan, Bora Oztekin, and Shuiwang Ji. GraphEBM: Molecular Graph Generation with Energy-Based Models. *arXiv preprint arXiv:2102.00546*, 2021.

Shiwei Liu, Tian Zhu, Milong Ren, Chungong Yu, Dongbo Bu, and Haicang Zhang. Predicting mutational effects on protein-protein binding via a side-chain diffusion probabilistic model. *Advances in Neural Information Processing Systems*, 36, 2024a.

Yijing Liu, Chao Du, Tianyu Pang, Chongxuan Li, Wei Chen, and Min Lin. Graph Diffusion Policy Optimization. *arXiv preprint arXiv:2402.16302*, 2024b.

Tianze Luo, Zhanfeng Mo, and Sinno Jialin Pan. Fast Graph Generation via Spectral Diffusion. *IEEE Transactions on Pattern Analysis and Machine Intelligence*, 2023.

Youzhi Luo, Keqiang Yan, and Shuiwang Ji. GraphDF: A Discrete Flow Model for Molecular Graph Generation. In *International conference on machine learning*, pp. 7192–7203. PMLR, 2021.

Tengfei Ma, Jie Chen, and Cao Xiao. Constrained Generation of Semantically Valid Graphs via Regularizing Variational Autoencoders. *Advances in Neural Information Processing Systems*, 31, 2018.

Manuel Madeira, Clement Vignac, Dorina Thanou, and Pascal Frossard. Generative modelling of structurally constrained graphs. *arXiv preprint arXiv:2406.17341*, 2024.

Giorgia Minello, Alessandro Bicciato, Luca Rossi, Andrea Torsello, and Luca Cosmo. Graph generation via spectral diffusion. *arXiv preprint arXiv:2402.18974*, 2024.

Chenhao Niu, Yang Song, Jiaming Song, Shengjia Zhao, Aditya Grover, and Stefano Ermon. Permutation Invariant Graph Generation via Score- Based Generative Modeling. In *International Conference on Artificial Intelligence and Statistics*, pp. 4474–4484. PMLR, 2020.

Long Ouyang, Jeffrey Wu, Xu Jiang, Diogo Almeida, Carroll Wainwright, Pamela Mishkin, Chong Zhang, Sandhini Agarwal, Katarina Slama, Alex Ray, et al. Training language models to follow instructions with human feedback. *Advances in neural information processing systems*, 35:27730–27744, 2022.

Hermina Petric Maretic, Mireille El Gheche, Giovanni Chierchia, and Pascal Frossard. Got: an optimal transport framework for graph comparison. *Advances in Neural Information Processing Systems*, 32, 2019.

Aram-Alexandre Pooladian, Heli Ben-Hamu, Carles Domingo-Enrich, Brandon Amos, Yaron Lipman, and Ricky TQ Chen. Multisample flow matching: Straightening flows with minibatch couplings. *arXiv preprint arXiv:2304.14772*, 2023.

Yiming Qin, Manuel Madeira, Dorina Thanou, and Pascal Frossard. Defog: Discrete flow matching for graph generation. *arXiv preprint arXiv:2410.04263*, 2024.

Raghunathan Ramakrishnan, Pavlo O Dral, Matthias Rupp, and O Anatole Von Lilienfeld. Quantum chemistry structures and properties of 134 kilo molecules. *Scientific data*, 1(1):1–7, 2014.

Milong Ren, Tian Zhu, and Haicang Zhang. Carbonnovo: Joint design of protein structure and sequence using a unified energy-based model. In *Forty-first International Conference on Machine Learning*, 2024. URL `https://openreview.net/forum?id=FSxTEvuFa7`.

Ida Schomburg, Antje Chang, Christian Ebeling, Marion Gremse, Christian Heldt, Gregor Huhn, and Dietmar Schomburg. Brenda, the enzyme database: updates and major new developments. *Nucleic acids research*, 32(suppl_1):D431–D433, 2004.

Prithviraj Sen, Galileo Namata, Mustafa Bilgic, Lise Getoor, Brian Galligher, and Tina Eliassi-Rad. Collective Classification in Network Data. *AI magazine*, 29(3):93–93, 2008.

Chence Shi, Minkai Xu, Zhaocheng Zhu, Weinan Zhang, Ming Zhang, and Jian Tang. GraphAF: a Flow-based Autoregressive Model for Molecular Graph Generation. In *International Conference on Learning Representations*, 2019.

Martin Simonovsky and Nikos Komodakis. GraphVAE: Towards Generation of Small Graphs Using Variational Autoencoders. In *Artificial Neural Networks and Machine Learning–ICANN 2018: 27th International Conference on Artificial Neural Networks, Rhodes, Greece, October 4-7, 2018, Proceedings, Part I 27*, pp. 412–422. Springer, 2018.

Daniel GA Smith, Lori A Burns, Andrew C Simmonett, Robert M Parrish, Matthew C Schieber, Raimondas Galvelis, Peter Kraus, Holger Kruse, Roberto Di Remigio, Asem Alenaizan, et al. PSI4 1.4: Open-source software for high-throughput quantum chemistry. *The Journal of chemical physics*, 152(18), 2020.

Yang Song, Jascha Sohl-Dickstein, Diederik P Kingma, Abhishek Kumar, Stefano Ermon, and Ben Poole. Score-Based Generative Modeling through Stochastic Differential Equations. In *International Conference on Learning Representations*, 2020.

Yuxuan Song, Jingjing Gong, Minkai Xu, Ziyao Cao, Yanyan Lan, Stefano Ermon, Hao Zhou, and Wei-Ying Ma. Equivariant Flow Matching with Hybrid Probability Transport for 3D Molecule Generation. *Advances in Neural Information Processing Systems*, 36, 2024.

Richard S Sutton, David McAllester, Satinder Singh, and Yishay Mansour. Policy Gradient Methods for Reinforcement Learning with Function Approximation. *Advances in neural information processing systems*, 12, 1999.

Alexander Tong, Jessie Huang, Guy Wolf, David Van Dijk, and Smita Krishnaswamy. Trajectorynet: A dynamic optimal transport network for modeling cellular dynamics. In *International conference on machine learning*, pp. 9526–9536. PMLR, 2020.

Alexander Tong, Nikolay Malkin, Guillaume Huguet, Yanlei Zhang, Jarrid Rector-Brooks, Kilian FATRAS, Guy Wolf, and Yoshua Bengio. Improving and Generalizing Flow-Based Generative Models with Minibatch Optimal Transport. In *ICML Workshop on New Frontiers in Learning, Control, and Dynamical Systems*, 2023.

Titouan Vayer, Laetitia Chapel, Rémi Flamary, Romain Tavenard, and Nicolas Courty. Optimal transport for structured data with application on graphs. *arXiv preprint arXiv:1805.09114*, 2018.

Clement Vignac, Igor Krawczuk, Antoine Siraudin, Bohan Wang, Volkan Cevher, and Pascal Frossard. Digress: Discrete denoising diffusion for graph generation. *arXiv preprint arXiv:2209.14734*, 2022.

Cédric Villani. Optimal Transport, volume 338 of. *Grundlehren der Mathematischen Wissenschaften [Fundamental Principles of Mathematical Sciences]*, pp. 71, 2009.

Hongwei Wang, Jia Wang, Jialin Wang, Miao Zhao, Weinan Zhang, Fuzheng Zhang, Xing Xie, and Minyi Guo. GraphGAN: Graph Representation Learning With Generative Adversarial Nets. In *Proceedings of the AAAI conference on artificial intelligence*, 2018.

Joseph L Watson, David Juergens, Nathaniel R Bennett, Brian L Trippe, Jason Yim, Helen E Eisenach, Woody Ahern, Andrew J Borst, Robert J Ragotte, Lukas F Milles, et al. De novo design of protein structure and function with RFdiffusion. *Nature*, 620(7976):1089–1100, 2023.

Zhe Xu, Ruizhong Qiu, Yuzhong Chen, Huiyuan Chen, Xiran Fan, Menghai Pan, Zhichen Zeng, Mahashweta Das, and Hanghang Tong. Discrete-state continuous-time diffusion for graph generation. *arXiv preprint arXiv:2405.11416*, 2024.

Qi Yan, Zhengyang Liang, Yang Song, Renjie Liao, and Lele Wang. Swingnn: Rethinking permutation invariance in diffusion models for graph generation. *arXiv preprint arXiv:2307.01646*, 2023.

Jason Yim, Andrew Campbell, Andrew YK Foong, Michael Gastegger, José Jiménez-Luna, Sarah Lewis, Victor Garcia Satorras, Bastiaan S Veeling, Regina Barzilay, Tommi Jaakkola, et al. Fast protein backbone generation with SE (3) flow matching. *arXiv preprint arXiv:2310.05297*, 2023.

Jiaxuan You, Rex Ying, Xiang Ren, William Hamilton, and Jure Leskovec. GraphRNN: Generating Realistic Graphs with Deep Auto-regressive Models. In *International conference on machine learning*, pp. 5708–5717. PMLR, 2018.

Chengxi Zang and Fei Wang. MoFlow: an invertible flow model for generating molecular graphs. In *Proceedings of the 26th ACM SIGKDD International Conference on Knowledge Discovery & Data Mining*, pp. 617–626, 2020.

Lingxiao Zhao, Xueying Ding, and Leman Akoglu. Pard: Permutation-invariant autoregressive diffusion for graph generation. *arXiv preprint arXiv:2402.03687*, 2024.

Tian Zhu, Milong Ren, and Haicang Zhang. Antibody design using a score-based diffusion model guided by evolutionary, physical and geometric constraints. In *Forty-first International Conference on Machine Learning*, 2024. URL `https://openreview.net/forum?id=1YsQIO4KaN`.

Yiheng Zhu, Zhenqiu Ouyang, Ben Liao, Jialu Wu, Yixuan Wu, Chang-Yu Hsieh, Tingjun Hou, and Jian Wu. Molhf: a hierarchical normalizing flow for molecular graph generation. In *Proceedings of the Thirty-Second International Joint Conference on Artificial Intelligence*, pp. 5002–5010, 2023.

Appendix

A Background

A.1 Continuous Flow Matching Generative Model

The generative model aims to establish a mapping $f : \mathbb{R}^d \to \mathbb{R}^d$ that transforms a noise distribution q_0 into a target data distribution q_1. This transformation is dependent on a density function p_0 over $\mathbb{R}^d$, and an integration map ψ_t, which induces a pushforward transformation $p_t = [\psi_t]_\#(p_0)$. This denotes the density of points $x \sim p_0$ transported from time 0 to time t along a vector field $u : [0, 1] \times \mathbb{R}^d \to \mathbb{R}^d$.

The vector field u is formulated as:

$$\mathrm{d}x = u_t(x)\mathrm{d}t.$$

The solution $\psi_t(x)$ to this ODE, with the initial condition $\psi_0(x) = x$, represents the trajectory of the point x governed by u from time 0 to time t.

The evolution of the density p_t, viewed as a function $p : [0, 1] \times \mathbb{R}^d \to \mathbb{R}$, is encapsulated by the continuity equation:

$$\frac{\partial p}{\partial t} = -\nabla \cdot (p_t u_t),$$

with the initial condition given by p_0. Here, u is the probability flow ODE for the path of marginal probabilities p, generated over time.

In practical applications, if the probability path $p_t(x)$ and the generating vector field $u_t(x)$ are known and $p_t(x)$ is tractably sampled, we leverage a time-dependent neural network $v_\theta(\cdot, \cdot) : [0, 1] \times \mathbb{R}^d \to \mathbb{R}^d$ to approximate u. The neural network is trained using the flow matching objective:

$$\mathcal{L}_{\mathrm{FM}}(\theta) = \mathbb{E}_{t\sim\mathcal{U}(0,1),x\sim p_t(x)}\|v_\theta(t, x) - u_t(x)\|^2, \tag{11}$$

which enhances the model's capability to simulate the target dynamics accurately. Avoiding the explicit construction of the intractable vector field, recent works express the probability path as a marginal over a joint involving a latent variable z: $p(x_t) = \int p(z)p_{t|z}(x_t|z)$. (Lipman et al., 2022; Tong et al., 2023) and the $p_{t|z}(x_t|z)$ is a conditional probability path, satisfying some boundary conditions at $t = 0$ and $t = 1$.

The conditional probability path also satisfies the transport equation with the conditional vector field $u_t(x|x_1)$:

$$\frac{\partial p_t(x|x_t)}{\partial t} = -\nabla \cdot (u_t(x|x_1)p_t(x_t|x_1)). \tag{12}$$

We can construct the marginal vector field $u_t(x)$ via the conditional probability path $p_{t|1}(x_t|x_1)$ as:

$$u_t(x) = \mathbb{E}_{x_1\sim p_{1|t}}[u_t(x|x_1)]. \tag{13}$$

We can replace the flow matching loss $\mathcal{L}_{\mathrm{FM}}$ with an equivalent loss regressing the conditional vector field $u_t(x|x_1)$ and marginalizing x_1 instead:

$$\begin{aligned}\mathcal{L}_{\mathrm{CFM}}(\theta) &= \mathbb{E}_{\mathcal{U}(t;0,1),x_1\sim q,x_t\sim p_t(x|x_1)}[u_\theta(t, x) - u_t(x|x_1)].\\ \nabla_\theta\mathcal{L}_{\mathrm{FM}}(\theta) &= \nabla_\theta\mathcal{L}_{\mathrm{CFM}}(\theta).\end{aligned}$$

So we can use $\mathcal{L}_{\mathrm{CFM}}(\theta)$ instead to train the parametric vector field u_θ.

B Related Works

B.1 Comparison with Discrete Flow Matching

Campbell et al. (2024) first introduced flow matching in discrete spaces using a continuous-time Markov chain. Building on this, Gat et al. (2024) expanded the framework to encompass general source and target couplings,

including U-coupling and C-coupling. GGFlow advances discrete flow matching and its source-target coupling to suit graph-structured data. Our approach innovatively incorporates efficient optimal transport for graphs within the flow matching framework. To address the inherent sparsity and permutation invariance of graphs, we employ a tailored prior distribution. Additionally, we implement an edge-augmented graph transformer to enhance generative performance and adopt a goal-guided framework for conditional generation. These advancements collectively enhance the practical applicability of GGFlow.

B.2 Comparison with Graph Discrete Diffusion Model

DiGress (Vignac et al., 2022) and PPGN (Haefeli et al., 2022) were among the first to apply discrete diffusion models to graph generation, highlighting the advantages of discrete state spaces. DiGress further introduced an optimal prior distribution and global structural features specifically designed to enhance graph generation. Their forward and generative processes are expressed as:

$$q(G^t|G^0) = \mathrm{Cat}(G^t, p = G^0\bar{Q}_t), \text{ with } \bar{Q}_t = Q_1 Q_2 \dots Q_t, \tag{14}$$

$$q(G^{t-1}|G^t, G^0) = \frac{q(G^t|G^{t-1}, G^0)q(G^{t-1}|G^0)}{q(G^t|G^0)} = \mathrm{Cat}(G^{t-1}; p = \frac{G^t Q_t^T \odot G^0 \bar{Q}_{t-1}}{G^0 \bar{Q}_t G^{t*}}), \tag{15}$$

where G^t represents the noisy graph at time t, and Q_t is the time-dependent transition matrix. These methods require maintaining convergence properties of the transition matrix and cumulative matrix products, constraining the choice of prior distributions and destabilizing training. In contrast, GGFlow employs a simpler interpolation between the prior and data distributions during training, avoiding cumulative products and improving both training stability and the ease of selecting appropriate priors.

B.3 Comparison with Graph Discrete Flow Model

GraphDF (Luo et al., 2021) uses a discrete flow model to generate molecular graphs by sequentially sampling discrete latent variables and mapping them to nodes and edges via invertible modulo-shift transforms. GGFlow simplifies this by transforming the invertible modulo-shift into a conditional vector field that interpolates between the prior and data distributions, bypassing the need for complex invertible mappings. Furthermore, while GraphDF adopts an autoregressive process for graph generation, GGFlow generates the entire graph in a one-shot manner, capturing holistic relationships among nodes and edges more efficiently.

B.4 Comparison with Graph Flow Matching Models

CatFlow (Eijkelboom et al., 2024) employs variational inference to apply flow matching to categorical data, but it only considers the conditional vector field under the assumption of independent coupling in the joint distribution $\pi(G^0, G^1)$ and fails to consider the inherent sparsity of graph structures. and DeFoG (Qin et al., 2024) also applies the discrete flow matching to establish the generation process of the graph, while they don't consider the generalization of the joint distribution. GGFlow extends this by generalizing $\pi(G^0, G^1)$ as an efficient 2-Wasserstein optimal transport map and incorporating an optimal prior distribution tailored for graph structures, improving performance in generation tasks. Additionally, GGFlow introduces a novel goal-directed approach for discrete flow matching in conditional generation tasks, enhancing its practical applicability.

B.5 Relationship to DiGress

DiGress and GGFlow are both generative models that share similar training objectives, specifically denoiser prediction. In contrast, their mathematical derivations and conceptual starting points differ.

DiGress, a diffusion model, is trained to predict the original data point (G^0) from a noisy version (G^t). Its training objective, $\mathcal{L}_{\text{DiGress}}$, is derived from the evidence lower bound (ELBO) of the data likelihood, which is gradually loosened to a permutation-invariant loss, as detailed in Lemma 3.2 of Vignac et al. (2022). The objective is defined as:

$$\mathcal{L}_{\text{DiGress}} = \mathbb{E}_{p_{\text{data}}(G^0)q_{t|0}(G^t|G^0)}(\log p_\theta(G|G^t))$$

$$\mathbb{E}_{p_{\text{data}}(G^0)}(-\log p_\theta(G^0)) \leq \mathcal{L}_{\text{DT}} \leq \sum_{k=1}^{T} \mathbb{E}_{p_{\text{data}}(G^0)q_{k|0}(G^k|G^0)}(-\log p_\theta(G|G^k)).$$

$$\begin{aligned}\mathcal{L}_{\text{DT}}(\theta) =& \mathbb{E}_{p_{\text{data}}(G_0)}\left[\text{KL}(q_{K|0}(G^K|G^0)||p_{\text{ref}}(G^K)) - \mathbb{E}_{q_{1|0}(G^1|G^0)}\left[\log p_\theta^{0|1}(G^0|G^1)\right]\right.\\ &\left. + \sum_{k=1}^{K-1} \mathbb{E}_{q_{k+1|0}(G^{k+1}|G^0)}\left[\text{KL}(q_{k|k+1,0}(G^k|G^{k+1},G^0)||p^\theta_{k|k+1}(G^k|G^{k+1}))\right]\right]\end{aligned}$$

The full derivation of the training objective and inequality, detailed in Proposition 9 in Campbell et al. (2022), shows how the ELBO is manipulated to arrive at this loss function.

GGFlow, a flow-matching model, also uses a denoiser prediction objective, but its derivation is rooted in different principles. The training objective, $\mathcal{L}_{\text{GGFlow}}$, is derived from an ELBO of the flow-matching process, as detailed in Section C.2 of Campbell et al. (2024):

$$\mathcal{L}_{\text{GGFlow}} = \mathbb{E}_{p_{\text{data}}(G^1)\mathcal{U}(t;0,1)\pi(G^0,G^1)p_t(G^t|G^0,G^1)}[\log \hat{p}_{1|t}(G^1|G^t,G^0)]$$

$$\mathbb{E}_{p_{\text{data}}(G^1)}(-\log p_\theta(G^1)) \leq -\mathcal{L}_{\text{ELBO}} = -(\mathcal{L}_{\text{GGFlow}} + \mathcal{L}_R + \mathcal{L}_{\text{KL}} + C) \leq -(\mathcal{L}_{\text{GGFlow}} + \mathcal{L}_R + C).$$

$$\mathcal{L}_{\text{R}} = \mathbb{E}_{\mathcal{U}(t;0,1)p_t(G^t)}[-R_t^\theta(G^t) + \mathbb{E}_{p_{1|t}(G^1|G^t)}[R_t(G^t|G^1)]\log R_t^\theta(G^t)]$$

Unlike DiGress, the GGFlow ELBO includes an additional term, $\mathcal{L}_R$. As argued in Section C.2 of Campbell et al. (2024), this term is often deemed unnecessary as it encourages the generative rate to match a chosen jump rate, simplifying the final training objective to just $\mathcal{L}_{\text{GGFlow}}$. Fortunately, this simplified training objective also satisfies permutation invariance, a shared desirable property with DiGress.

C Proofs

C.1 Optimal Prior Distribution

This prior is structured as a product of a single distribution v for all nodes and a single distribution e for all edges, $\prod_i v \times \prod_{i,j} e$, to ensure exchangeability across the graph components.

Theorem 2 (Optimal prior distribution)**.** *Consider the class $\mathcal{C} = \{\prod_i u \times \prod_{i,j} v, (u,v) \in \mathcal{P}(\mathcal{V}) \times \mathcal{P}(\mathcal{E})\}$ of distributions over graphs, which factorize as the product of a uniform distribution v over node attribute space $\mathcal{V}$ and a uniform distribution e over edge attribute space $\mathcal{E}$. Given any arbitrary distribution P over graphs (viewed as a tensor of order $n+n^2$), with q_V and q_E as its marginal distributions for node and edge attributes respectively, then the orthogonal projection of P onto $\mathcal{C}$ is defined as $\phi^G = \prod_i q_V \times \prod_{i,j} q_E$. This projection minimizes the Euclidean distance:*

$$\phi^G \in \arg\min_{(v,e)\in\mathcal{C}} \|P - \prod_{1\leq i\leq n} v \times \prod_{1\leq i,j\leq n} e\|_2^2.$$

The details and proof of Theorem 2 are extensively discussed in DiGress (Vignac et al., 2022).

C.2 Choice of conditional velocity field

This section first demonstrates that the marginal vector field $u_t(G, G^t)$ in Equation 3 satisfies the Kolmogorov equation, which corresponds to the Continuity equation in continuous space, provided the conditional vector field $u_t(G^t, G|G^1, G^0)$ also satisfies it.

Proposition 3. *If $u_t(G^t, G|G^1, G^0)$ is a conditional vector field that satisfies the conditional Kolmogorov equation $\partial_t p_{t|1}(G^t|G^1, G^0) = \sum_{G\neq G^t} u_t(G, G^t|G^1, G^0)p_{t|1}(G|G^1, G^0) - \sum_{G\neq G^t} u_t(G^t, G|G^1, G^0)p_{t|1}(G^t|G^1, G^0)$, then vector field*

$$u_t(G, G^t) = \mathbb{E}_{p_{1|t}(G^1,G^0|G)}(u_t(G, G^t|G^0, G^1)) \tag{16}$$

also satisfies the Kolmogorov equation $\partial_t p_t(G^t) = \sum_{G \neq G^t} u_t(G, G^t) p_{t|1}(G) - \sum_{G \neq G^t} u_t(G^t, G) p_{t|1}(G^t)$.

Proof. We use the fact that $u_t(G, G) = -\sum_{G^i \neq G^j} u_t(G^i, G^j)$ for compactness and denote the joint distribution of G^0 and G^1 as $\pi(G^0, G^1)$:

$$
\begin{aligned}
\partial_t p_{t|1}(G^t|G^1, G^0) &= \sum_G u_t(G, G^t|G^1, G^0) p_{t|1}(G|G^1, G^0) \\
\mathbb{E}_{\pi(G^1,G^0)}[\partial_t p_{t|1}(G^t|G^1, G^0)] &= \mathbb{E}_{\pi(G^1,G^0)}[\sum_G u_t(G, G^t|G^1, G^0) p_{t|1}(G|G^1, G^0)] \\
\partial_t \mathbb{E}_{\pi(G^1,G^0)}[p_{t|1}(G^t|G^1, G^0)] &= \sum_G \sum_{(G^0,G^1)} \pi(G^0, G^1) u_t(G, G^t|G^1, G^0) p_{t|1}(G|G^1, G^0) \\
\partial_t p_t(G^t) &= \sum_G \sum_{(G^0,G^1)} p_{1|t}(G^1, G^0|G) u_t(G, G^t|G^1, G^0) p_t(G) \quad \text{based on Bayes Rule} \\
\partial_t p_t(G^t) &= \sum_G [\sum_{(G^0,G^1)} p_{1|t}(G^1, G^0|G) u_t(G, G^t|G^1, G^0)] p_t(G) \\
\partial_t p_t(G^t) &= \sum_G u_t(G, G^t) p_t(G)
\end{aligned}
$$

Therefore, we have proven that $u_t(G, G^t)$ also satisfies the Kolmogorov equation. □

We then prove that the proposed conditional vector field,

$$
u_t(G, G^t|G^0, G^1) = \frac{\mathrm{ReLU}(\partial_t p_{t|1}(G|G^1, G^0) - \partial_t p_{t|1}(G^t|G^1, G^0))}{\mathbf{Z}_t \cdot p_{t|1}(G^t|G^1, G^0)}
$$

satisfies the conditional Kolmogorov equation. where $\mathrm{ReLU(a)} = \max(\mathrm{a}, 0)$ and $\mathbf{Z}_t = |\{G^t : p_t(G^t|G^0, G^1) > 0\}|$. $u_t(G, G^t|G^0, G^1) = 0$ when $p_t(G|G^1, G^0) = 0$ and $p_t(G^t|G^1, G^0) = 0$. When $G^t = G$, the conditional vector field $u_t(G^t, G^t|G^0, G^1) = -\sum_{G^t \neq G} u_t(G^t, G|G^0, G^1)$. We assume that if $p_{t|1}(G|G^1, G^0) = 0$, then $\partial_t p_{t|1}(G|G^1, G^0) = 0$.

Proof. The proof proceeds by verifying that the conditional Kolmogorov equation is satisfied.

We first consider the case where $p_{t|1}(G^t|G^1, G^0) > 0$. The right-hand side (RHS) of the Kolmogorov equation is:

$$
\begin{aligned}
\mathbf{RHS} = & \sum_{G \neq G^t, p_{t|1}(G|G^1,G^0)>0} \frac{\mathrm{ReLU}(\partial_t p_{t|1}(G^t|G^1,G^0) - \partial_t p_{t|1}(G|G^1,G^0))}{\mathbf{Z}_t \cdot p_{t|1}(G|G^1,G^0)} p_{t|1}(G|G^1,G^0) \\
& - \sum_{G \neq G^t, p_{t|1}(G|G^1,G^0)>0} \frac{\mathrm{ReLU}(\partial_t p_{t|1}(G|G^1,G^0) - \partial_t p_{t|1}(G^t|G^1,G^0))}{\mathbf{Z}_t \cdot p_{t|1}(G^t|G^1,G^0)} p_{t|1}(G^t|G^1,G^0) \\
= & \frac{1}{\mathbf{Z}_t} \sum_{G \neq G^t, p_{t|1}(G|G^1,G^0)>0} \mathrm{ReLU}(\partial_t p_{t|1}(G^t|G^1,G^0) - \partial_t p_{t|1}(G|G^1,G^0)) \\
& - \frac{1}{\mathbf{Z}_t} \sum_{G \neq G^t, p_{t|1}(G|G^1,G^0)>0} \mathrm{ReLU}(\partial_t p_{t|1}(G|G^1,G^0) - \partial_t p_{t|1}(G^t|G^1,G^0)) \\
= & \frac{1}{\mathbf{Z}_t} \sum_{G \neq G^t, p_{t|1}(G|G^1,G^0)>0} (\partial_t p_{t|1}(G^t|G^1,G^0) - \partial_t p_{t|1}(G|G^1,G^0)) \\
= & \frac{\mathbf{Z}_t - 1}{\mathbf{Z}_t} \partial_t p_{t|1}(G^t|G^1,G^0) - \frac{1}{\mathbf{Z}_t} \sum_{G \neq G^t, p_{t|1}(G|G^1,G^0)>0} \partial_t p_{t|1}(G|G^1,G^0) \\
= & \frac{\mathbf{Z}_t - 1}{\mathbf{Z}_t} \partial_t p_{t|1}(G^t|G^1,G^0) - \frac{1}{\mathbf{Z}_t} \partial_t (1 - p_{t|1}(G^t|G^1,G^0)) \\
= & \frac{\mathbf{Z}_t - 1}{\mathbf{Z}_t} \partial_t p_{t|1}(G^t|G^1,G^0) + \frac{1}{\mathbf{Z}_t} \partial_t p_{t|1}(G^t|G^1,G^0) \\
= & \partial_t p_{t|1}(G^t|G^1,G^0) = \mathbf{LHS}
\end{aligned}
$$

For the case where $p_{t|1}(G^t|G^1, G^0) = 0$, our initial assumption states that $\partial_t p_{t|1}(G^t|G^1, G^0) = 0$. Due to the structure of the vector field, both $u_t(G^t, G|G^1, G^0)$ and $u_t(G, G^t|G^1, G^0)$ will also be zero. Therefore, both sides of the Kolmogorov equation equal zero, and the equation is satisfied. □

Finally we can simplify the conditional vector field as:

$$
\begin{aligned}
u_t(G, G^t|G^0, G^1) &= \frac{\mathrm{ReLU}(\partial_t p_{t|1}(G|G^1) - \partial_t p_{t|1}(G^t|G^1))}{\mathbf{Z}_t \cdot p_{t|1}(G^t|G^1)} \\
&= \frac{1}{\mathbf{Z}_t (1-t) p_{\mathrm{ref}}} \delta\{G, G^1\}(1 - \delta\{G^t, G^1\}), G_t \neq G,
\end{aligned}
$$

where $\mathrm{ReLU(a)} = \max(\mathrm{a}, 0)$ and $\mathbf{Z}_t = |\{G^t : p_t(G^t|G^0, G^1) > 0\}|$. $u_t(G, G^t|G^0, G^1) = 0$ when $p_t(G|G^1, G^0) = 0$ and $p_t(G^t|G^1, G^0) = 0$. When $G^t = G$, the conditional vector field $u_t(G^t, G^t|G^0, G^1) = -\sum_{G^t \neq G} u_t(G^t, G|G^0, G^1)$.

Proof. Consider the conditional probability $p_{t|1}(G^t|G^1, G^0) = p_t(G^t|G^1, G^0) = \mathrm{Cat}\Big(t\delta\{G^1, G^t\} + (1-t)p_{\mathrm{ref}}\Big)$, where p_{ref} is the prior distribution. We derive its time derivative:

$$
\partial_t p_{t|1}(G^t|G^1, G^0) = \delta\{G^1, G^t\} - p_{\mathrm{ref}}, \tag{17}
$$

We then construct the conditional rate matrix $u_t(G^t, G|G^1, G^0)$ as:

$$
\begin{aligned}
u_t(G^t, G|G^1, G^0) &= \frac{\mathrm{ReLU}(\partial_t p_{t|1}(G|G^1,G^0) - \partial_t p_{t|1}(G^t|G^1,G^0))}{\mathbf{Z}_t \cdot p_{t|1}(G^t|G^1,G^0)} \\
&= \frac{\mathrm{ReLU}(\delta\{G, G^1\} - p_{\mathrm{ref}} - \delta\{G^t, G^1\} + p_{\mathrm{ref}})}{\mathbf{Z}_t (t\delta\{G^1, G^t\} + (1-t)p_{\mathrm{ref}})} \\
&= \frac{\mathrm{ReLU}(\delta\{G, G^1\} - \delta\{G^t, G^1\})}{\mathbf{Z}_t (t\delta\{G^1, G^t\} + (1-t)p_{\mathrm{ref}})}.
\end{aligned}
$$

The expression simplifies under the assumption that $G^t \neq G$. The only non-zero values occur when $G = G^1$ and $G^t \neq G^1$, thus yielding:

$$u_t(G^t, G|G^1) = \frac{1}{\mathbf{Z}_t(1-t)q_G}\delta\{G, G^1\}(1 - \delta\{G^t, G^1\}), G^t \neq G. \tag{18}$$

where $\mathbf{Z}_t = |\{G^t : p_t(G^t|G^1, G^0) > 0\}|$. □

C.3 Proof of Proposition 1

Proof. The Kolmogorov forward equations for discrete flow matching are expressed as:

$$\partial_t p_t = u_t p_t, \tag{19}$$

If we establish the permutation invariance of the prior distributions p_{ref} and the permutation equivariance of conditional flow probabilities, then it follows that $p(G^1)$ is permutation exchangeable.

According to the Theorem 2, we deduce the permutation invariance of the prior distribution p_{ref}. Given the conditional probabilities $p(G^{t+\Delta t}|G^t) = \text{Cat}\Big(\delta\{G^t, G^{t+\Delta t}\} + \hat{u}_t(G^t, G^{t+\Delta t})\Delta t\Big)$, it suffices to demonstrate the permutation equivariance of the conditional probabilities. This requires showing the permutation equivariance of the vector field u_t. Consider the case for nodes:

$$\begin{aligned}
\pi u_t^V(V_i^t, V_i^{t+\Delta t}) &= \pi\left(\mathbb{E}_{\hat{p}^V_{1|t}(V_i^1|V_i^t)}[u_t^V(V_i^t, V_i^{t+\Delta t}|V_i^1, V_i^0)]\right), \\
\text{LHS} &= u_t^V(V^t_{\pi^{-1}(i)}, V^{t+\Delta t}_{\pi^{-1}(i)}), \\
\text{RHS} &= \left(\mathbb{E}_{\hat{p}^V_{1|t}(V^1_{\pi^{-1}(i)}|V^t_{\pi^{-1}(i)})}[u_t^V(V^t_{\pi^{-1}(i)}, V^{t+\Delta t}_{\pi^{-1}(i)}|V^1_{\pi^{-1}(i)}, V^0_{\pi^{-1}(i)})]\right), \\
&= u_t^V(V^t_{\pi^{-1}(i)}, V^{t+\Delta t}_{\pi^{-1}(i)}) = \text{LHS}.
\end{aligned}$$

where π is a permutation operator. This establishes the permutation equivariance of u_t and the exchangeability of the generated distribution. □

C.4 Proof of Theorem 1

First, we want to clarify the rationale and foundation of our theorem. The goal of optimal transport is to pair source and target data points with minimal cost during training, which is beneficial for our interpolation (Bose et al., 2023; Song et al., 2024). Thus, we design our optimal transport approach from the perspective of interpolation.

We define the node order of the graph G as the order of the nodes and edges in matrix representation. For example, if the node set of G is $\{A, B, C\}$, the possible node orders include (A, B, C), (B, A, C) or (C, B, A).

In the interpolation process, we transform the graph representation to a matrix representation before performing interpolation. For example, for source data $G^0 = (V^0, E^0), V^0 \in \mathbb{R}^{a\times n}, E^0 \in \mathbb{R}^{a\times a\times m}$ and target data $G^1 = (V^1, E^1), V^1 \in \mathbb{R}^{a\times n}, E^1 \in \mathbb{R}^{a\times a\times m}$, where a is the number of nodes, n is the class number of nodes, and m is the class number of edges, the node orders of G^0 and G^1 have been fixed. Therefore, interpolation is performed directly on these fixed node orders.

The optimal transport aims to find pairs with the minimum cost for interpolation, and the interpolation is conducted on a fixed node order. Additionally, during optimal transport calculations, we also utilize the matrix representation of these graphs and our prior distribution is permutation invariant. Therefore, we aim to match source data with the target data G^1 whose node order is fixed, to achieve minimal transport cost. Furthermore, we assume that all pairs of source and target data share the same node order during optimal transport, which also facilitates the identification of pairs with minimal cost.

Regarding the permutation of the intermediate graph G^t, we have $\pi G^t = t\pi G^0 + (1-t)\pi G^1$, where G^0 and G^1 share an identical permutation. Our network $\hat{p}^1(G^1|G^0, G^t)$ needs to maintain permutation equivariance, such that $\hat{p}^1(G^1|\pi G^0, \pi G^t) = \pi\hat{p}^1(G^1|G^0, G^t)$ for any permutation π to approximate πG^1. So we prove the invariance of optimal transport under identical permutations, i.e. $\phi(G^0, G^1) = \phi(\pi G^0, \pi G^1)$.

Proof. Building on the foundations established in Theorem 2 and Proposition 1, we confirm the permutation invariance of both the target and source distributions. The Hamming distance is invariance under identical permutations π, as shown by:

$$\begin{aligned} H(G^0, G^1) &= \sum_i \delta(v_i^0, v_i^1) + \frac{1}{2}\sum_{i,j} \delta(e_{ij}^0, e_{ij}^1) \\ &= \sum_i \delta(v_{\pi^{-1}(i)}^0, v_{\pi^{-1}(i)}^1) + \frac{1}{2}\sum_{i,j} \delta(e_{\pi^{-1}(i)\pi^{-1}(j)}^0, e_{\pi^{-1}(i)\pi^{-1}(j)}^1) \\ &= H(\pi G^0, \pi G^1) \end{aligned}$$

This property of the Hamming distance ensures the invariance of the optimal transport map ϕ^* under identical permutations.

□

Additionally, the prior distribution is permutation invariant and our GraphEvo is permutation equivariance, all permutations of graphs are generated with equal probability (Eijkelboom et al., 2024).

Lemma 1. *Let $p_0(G)$ be an exchangeable distribution and our model $\hat{p}_{1|t}(G^1|G^t, G^0)$ is permutation equivariant. Then, all permutations of generated graphs with equal probability.*

Proof. As the permutation equivariance of our model $\hat{p}_{1|t}(G^1|G^t, G^0)$, implies the equivariance of our vector fields u_t. Moreover, the sampling procedure exhibits permutation equivariance, where π is a permutation.

$$\begin{aligned} &\hat{p}_{1|t}(G^1|\pi G^0) = \pi \hat{p}_{1|t}(G^1|G^0), \quad t = 0 \\ &p_{\Delta t|0}(G^{\Delta t}|\pi\hat{G}^1, \pi G^0) = \delta\{\cdot, \pi G^0\} + u_0(\cdot, \pi G^0|\pi G^0, \pi\hat{G}^1)\Delta t \\ &= \pi[\delta\{\cdot, G^0\} + u_0(\cdot, G^0|G^0, \hat{G}^1)\Delta t] = \pi p_{\Delta t|0}(G^{\Delta t}|\hat{G}^1, G^0), \quad t = 0 \\ &p_{t+\Delta t|t}(G^{\Delta t+t}|\pi\hat{G}^1, \pi G^t, \pi G^0) = \delta\{\cdot, \pi G^t\} + u_t(\cdot, \pi G^t|\pi G^0, \pi\hat{G}^1)\Delta t \\ &= \pi[\delta\{\cdot, G^t\} + u_t(\cdot, G^t|G^0, \hat{G}^1)\Delta t] = \pi p_{t+\Delta t|t}(G^{\Delta t+t}|\hat{G}^1, G^t, G^0), \quad t = \Delta t, \ldots, 1 - \Delta t \end{aligned}$$

Therefore, since p_0 assigns equal density of all permutations of G, the resulting distribution p_1 preservers this property. □

D Details of GraphEvo

GraphEvo is a novel edge-augmented graph transformer model designed for graph data. To enhance the generative capabilities of GGFlow, GraphEvo introduces a triangle update mechanism, which significantly improves the exchange of edge information. We incorporate FiLM and PNA layers into our architecture (Vignac et al., 2022):

$$\begin{aligned} \text{FiLM}(X_1, X_2) &= X_1(\text{Linear}(X_2) + 1) + \text{Linear}'(X_2) \\ \text{PNA}(X) &= \text{Linear}\Big(\text{Cat}(\max(X), \min(X), \text{mean}(X), \text{std}(X))\Big). \end{aligned}$$

The full architecture of GraphEvo is illustrated in Algorithm 3 and is permutation equivariant. The time complexity of GraphEvo is $O(N^3)$.

GraphEvo integrates global structural features to improve generation performance, including both graph-theoretic and domain-specific attributes:

Graph-theoretic features: These encompass node-level properties such as the number of k-cycles ($k \leq 5$) containing this point and an estimate of the largest connected component, alongside graph-level metrics like the total number of k-cycles ($k \leq 6$) and connected components.

Algorithm 3 Architecture of GraphEvo

Require: G, t, N_{layer}
$\mathbf{V}, \mathbf{E} \leftarrow G$
$\mathbf{y} \leftarrow \text{ExtractFeature}(G), \mathbf{t} \leftarrow \text{TimeEmbedding}(t)$
$\mathbf{y} \leftarrow \mathbf{y} + \mathbf{t}$
$\mathbf{X}, \mathbf{E}, \mathbf{y} \leftarrow \text{Linear}(V), \text{Linear}(\mathbf{E}), \text{Linear}(\mathbf{y})$
for $t = 0, 1, \ldots, N_{\text{layer}}$ **do**
  $\mathbf{X}', \mathbf{E}', \mathbf{y}' \leftarrow \text{SelfAttention}(\mathbf{X}, \mathbf{E}, \mathbf{y})$
  $\mathbf{X} \leftarrow \text{ReLU}\Big(\text{LayerNorm}(\mathbf{X} + \text{Dropout}(\mathbf{X}'))\Big)$
  $\mathbf{E} \leftarrow \text{ReLU}\Big(\text{LayerNorm}(\mathbf{E} + \text{Dropout}(\mathbf{E}'))\Big)$
  $\mathbf{y} \leftarrow \text{ReLU}\Big(\text{LayerNorm}(\mathbf{y} + \text{Dropout}(\mathbf{y}'))\Big)$
end for
$\hat{p}^V_{1|t}(V^1|V^t, V^0), \hat{p}^E_{1|t}(E^1|E^t, E^0), \mathbf{y} \leftarrow \text{Linear}(V), \text{Linear}(\mathbf{E}), \text{Linear}(\mathbf{y})$
return $\hat{p}^V_{1|t}(V^1|V^t, V^0), \hat{p}^E_{1|t}(E^1|E^t, E^0), \mathbf{y}$

Molecular features: These account for the current valency of each atom and the molecular weight of the entire molecule.

D.1 Proof of Proposition 2

Proof. Let $G^t = (V^t, E^t)$ is a intermediate graph, and $\pi G^t = (\pi^* V, \pi^* E \pi)$ is the permutation. To prove the permutation properties of the graph, we need to consider two aspects: additional structural features and the model architecture.

First, the spectral and structural features are permutation equivariant for node-level features and invariant for graph-level features. Additionally, the FiLM blocks and Linear layers are permutation equivariant, while the PNA pooling function is permutation invariant. Layer normalization is also permutation equivariant.

As GraphEvo is built using permutation equivariant components, we conclude that the overall model is permutation equivariant.

□

E Analysis of Optimal Transport

To analyze the time complexity of optimal transport (OT), we compared the training time of OT with that of DiGress, using identical architectures on an NVIDIA A100 80G GPU. We evaluated the effects of model size, batch size, and number of nodes by measuring the duration of single training steps across three different datasets. Our results indicate that the time required for OT accounts for only 5% of the total training time, highlighting the efficiency of our optimal transport.

Table S1: Time Complexity of Optimal Transport

Dataset	Planar	Zinc250k	Community-small
DiGress Training Time (s)	0.1647	0.1690	0.0456
GGFlow Training Time (s)	0.1264	0.1301	0.0408
Optimal Transport Time (s)	0.0025	0.0070	0.0024
Percentage of OT	1.9%	5.3%	5.6%
Model Size (M)	3.6	4.6	6.4
Batch Size	64	128	80
Number of Nodes	64	[6,38]	[12,20]

To further demonstrate the advantages of our proposed distance metric, we conducted a comparative analysis using Fused-Gromov-Wasserstein (FGW), which is defined in Vayer et al. (2018), as an alternative permutation-invariant graph distance for model training.

A primary challenge encountered with FGW was its computational overhead. We observed that calculating the FGW distance on both the Community-small and ZINC250k datasets required several orders of magnitude more time than our model's typical training duration. As detailed in Table S2, the computation time for FGW on ZINC250k was particularly prohibitive, preventing us from completing a full training run for a comparative model. Consequently, a comprehensive model trained with FGW was only feasible on the Community-small dataset.

Table S2: Time comparison of Optimal Transport distance computation

Dataset	Zinc250k	Community-small
Hamming Distance Training Time (s)	0.0070	0.0024
Fused Gromov-wasserstein Distance Training Time (s)	60.3062	9.0301

Table S3 presents the generative performance comparison on the Community-small dataset. Our model, utilizing the Hamming distance, outperformed the FGW-based model on the Cluster and Orbit metrics, while exhibiting a slightly reduced performance on the Degree metric.

Table S3: Generative results with different Optimal Transport distances on Community-small dataset

Method	Degree	Cluster	Orbit
Hamming Distance	0.011	0.030	0.002
Fused Gromov-wasserstein Distance	0.004	0.069	0.006

More critically, our model demonstrated superior training stability compared to the FGW-based model, as evidenced by the validation KL divergence on the validation set. Figure S1 illustrates this enhanced stability. This improved stability is directly attributable to our distance metric being specifically tailored and better adapted to the Flow Matching training methodology.

These findings collectively indicate that, while our proposed optimal transport approach limits invariance to identical permutations, it does not negatively impact the model's practical performance and is better suited and more efficient for our Flow Matching model than Fused-Gromov-Wasserstein.

F Toy example of goal-guided graph generation

We demonstrate the utility of our goal-guided framework of flow matching with a toy example, depicted in Figure S2: (a) shows a trained unconditional flow matching model mapping noise distribution p_0 to data distribution p_1. (b, c) illustrate the effect of temperature T on the exploration, with higher temperatures resulting in broader data point distribution. (d) shows how fine-tuning according to Equation 10 concentrates data in regions with higher rewards. (e-f) illustrate the corresponding flow matching trajectories.

G Additional Experiments Results

In this section, we present additional metrics including Spectre (Spec.) and Validity&Novelty&Uniquess (Val.&Nov.&Uni.) across general graph datasets including the Planar and Enzymes datasets, as summarized in Tables S4, S5 and S6. The MMD kernel in the planar dataset followed the GruM (Jo et al., 2024). We also include the standard deviation of our results in Table S7, illustrating the consistency and superior performance of our method.

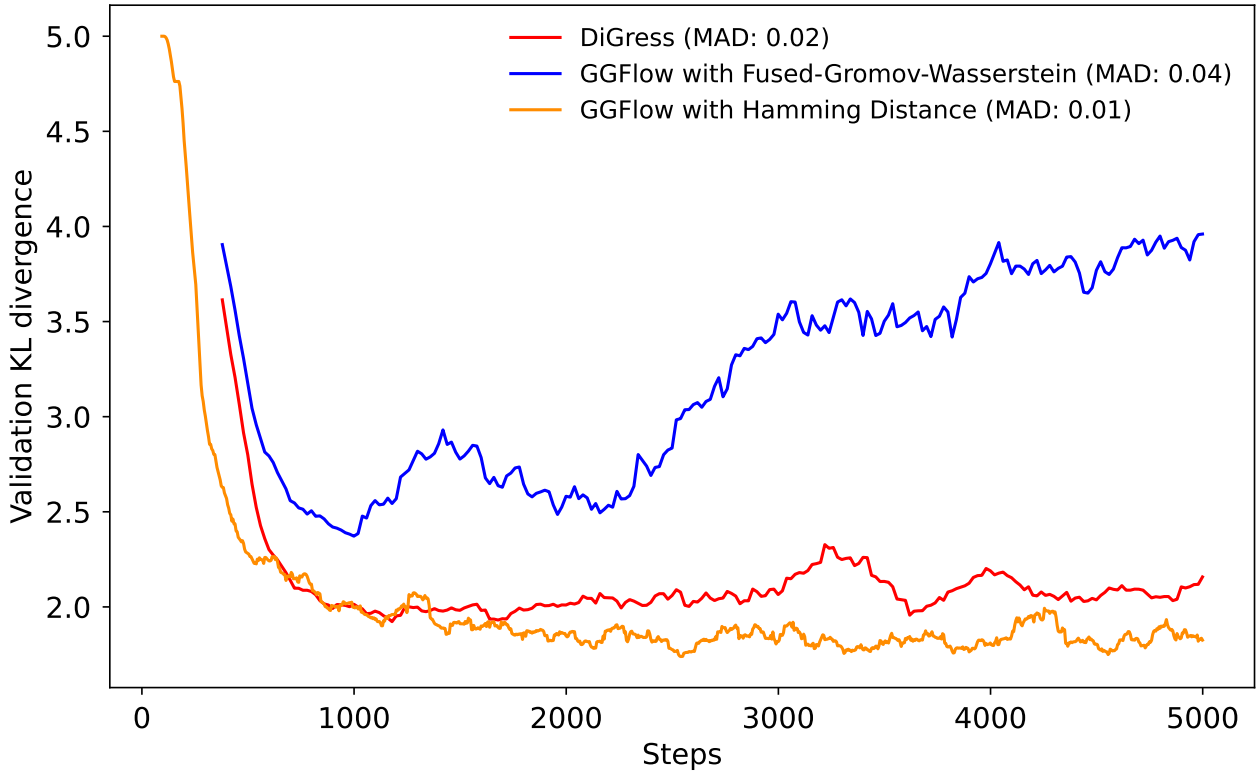

Figure S1: Validation KL Divergence comparison of different Optimal Transport approaches on Community-small dataset

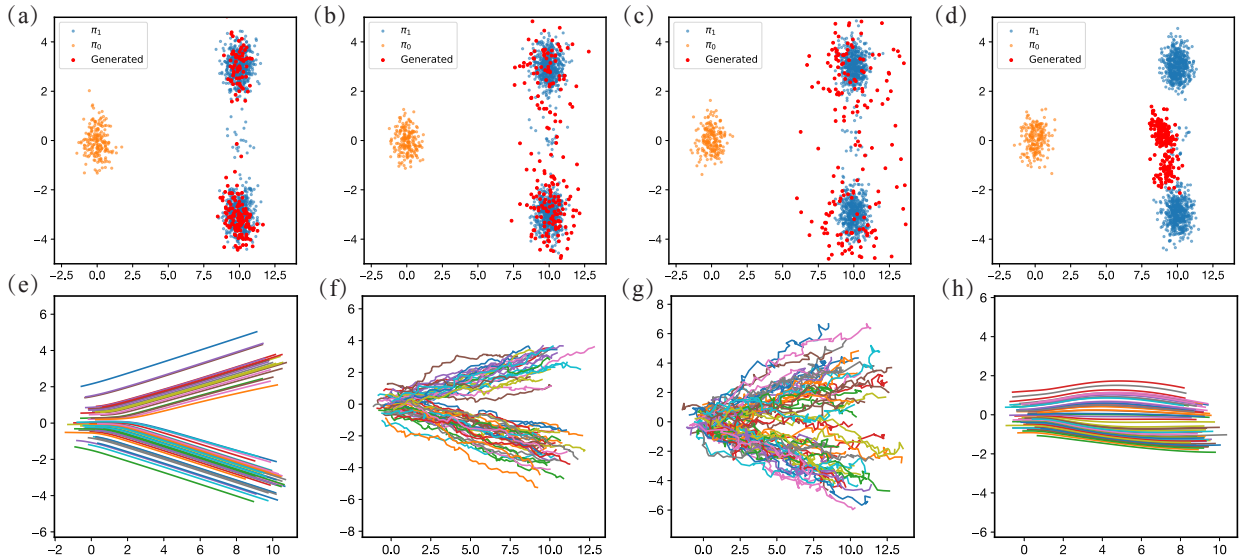

Figure S2: (a-d) Data distribution of the flow matching model, π_0 is the original distribution (orange), π_1 is the target data distribution (blue), and the red dots are the data distribution generated by the model. (e-h) In reinforcement learning, the flow matching model conducts exploration/sampling trajectories

To further compare GGFlow with baseline models, we measured the MMD between the test datasets and a set of 1,024 generated graphs in the Ego-small and Community-small datasets. The results in Table S8 demonstrate that GGFlow achieves the highest performance across all metrics, significantly outperforming other baseline models.

Table S4: Additional generation results on the generic graph datasets. Results are the means of 3 different runs. The best results are marked **bold**.

Method	**Ego-small**		**Community-small**		**Grid**		**Step**
	Spec.	Nov.&Uni.	Spec.	Nov.&Uni.	Spec.	Nov.&Uni.	
Training Set	0.006	30	0.012	100	0.009	25	-
GDSS	0.034	27.5	0.053	100.0	0.043	100.0	1000
GSDM	-	-	**0.024**	0.0	0.015	0.0	1000
DiGress	0.017	30.0	0.055	100.0	0.025	100.0	500
SwinGNN	0.016	**52.5**	0.025	55.0	**0.008**	100.0	500
GGFlow	**0.006**	32.5	0.031	**100.0**	0.022	**100.0**	500

Table S5: Generation results on the planar graph datasets. The best results are marked **bold**. σ denotes the standard deviation.

Method	**Planar**					**Step**
	Deg.	Clus.	Orbit	Spec.	Val.&Nov.&Uni.	
Training Set	0.0002	0.0165	0.0002	0.0050	100	-
GDSS	0.0039	0.2593	0.1732	0.0370	0.0	1000
GRASP	0.0022	0.2749	0.0055	0.0098	0.0	200
DiGress	**0.0003**	0.0372	0.0098	0.0106	75.0	500
GruM	0.0004	0.0382	0.0095	**0.0069**	87.5	1000
GGFlow	0.0156	**0.0196**	**0.0019**	0.0091	**97.5**	500
σ	0.0064	0.0037	0.0006	0.0012	2.5	-

Table S6: Generation results on the Enzymes graph datasets. The best results are marked **bold**. σ denotes the standard deviation.

Method	**Enzymes**				**Step**
	Deg.	Clus.	Orbit	Avg.	
Training Set	0.008	0.096	0.012	0.039	-
GraphRNN	0.017	0.043	0.021	0.043	-
GraphAF	1.669	1.283	0.266	1.073	-
GraphDF	1.503	1.061	0.202	0.922	-
GraphVAE	1.369	0.629	0.191	0.730	-
EDP-GNN	0.023	0.268	0.082	0.124	1000
GDSS	0.026	0.102	0.009	0.046	1000
GSDM	0.013	0.088	0.010	0.037	1000
DiGress	0.010	0.046	0.002	0.019	500
GGFlow	**0.008**	**0.026**	**0.002**	**0.012**	500
σ	0.0041	0.0106	0.0008	0.0130	-

Table S7: Standard deviation and mean of generation results on the general graph datasets. μ and σ denote the mean and standard deviation, respectively

Metric	**Ego-small**				**Community-small**				**Grid**			
	Deg.	Clus.	Orbit	Sepc.	Deg.	Clus.	Orbit	Sepc.	Deg.	Clus.	Orbit	Sepc.
μ	0.005	0.033	0.005	0.008	0.011	0.030	0.002	0.031	0.030	0.000	0.016	0.022
σ	0.007	0.012	0.003	0.001	0.006	0.012	0.002	0.002	0.008	0.000	0.003	0.001

Table S8: Generation results on the generic graph datasets with 1024 generated graphs. The best results are marked **bold**.

Method	**Ego-small**				**Community-small**				**Step**
	Deg.	Clus.	Orbit	Sepc.	Deg.	Clus.	Orbit	Spec.	
GraphRNN	0.040	0.050	0.060	-	0.030	0.010	0.010	-	-
GNF	0.010	0.030	0.001	-	0.120	0.150	0.200	-	-
EDP-GNN	0.010	0.025	0.003	-	0.006	0.127	0.018	-	1000
GDSS	0.023	0.020	0.005	0.047	0.029	0.068	0.004	0.151	1000
GSDM	-	-	-	-	**0.003**	0.008	0.0009	0.011	1000
DiGress	0.017	0.038	0.006	0.021	0.013	0.040	0.004	0.055	500
SwinGNN	0.004	0.023	0.003	0.023	0.003	0.088	0.010	0.016	500
GGFlow	**0.004**	**0.004**	**0.0008**	**0.009**	0.004	**0.003**	**0.0006**	0.018	500

H Implement Details

H.1 Algorithms of GGFlow

Details of the training procedure and guided training procedure are provided in Algorithm 4 and 5.

Algorithm 4 Training Procedure of GGFlow

Require: $G = (V, E), q_V, q_E,$

for $n \in \{0, \ldots, N_{\text{iter}} - 1\}$ **do**
  $t \in \mathcal{U}(0, 1), G^1 = G$
  $G^0 = (V^0, E^0) \sim p^{\text{ref}}$
  $(G^0, G^1) \sim \text{OptimalTransport}(G^0, G^1)$
  // Sample from conditional probability flow.
  $V^t = (t\delta\{V^1, \cdot\} + (1-t)V^0)$ and $E^t = (t\delta\{E^1, \cdot\} + (1-t)E^0)$
  $\hat{p}^V_{1|t}(V^1|V^t, V^0), \hat{p}^E_{1|t}(E^1|E^t, E^0), \mathbf{y} = \text{GraphEvo}_{\theta_n}(V^t, E^t, t, f^t)$
  $\mathcal{L} = \mathbb{E}_{p_{\text{data}}(G^1)\mathcal{U}(t;0,1)\pi(G^0,G^1)p_t(G^t|G^0,G^1)}[\log \hat{p}_{1|t}(G^1|G^t, G^0)]$
  $\theta_{n+1} = \text{optimizer_update}(\theta_{\text{n}}, \mathcal{L})$
end for
$\theta^* = \theta_{N_{\text{iter}}}$
return θ^*

H.2 Baselines Implementation

To benchmark the performance of GGFlow, we ensure consistency by using identical splits of training and test sets across all datasets. Below, we provide the implementation details for each baseline model. To guarantee a fair comparison, most baseline models are retrained three times, and the average results from these runs are reported as the final outcomes in unconditional generation tasks. The results of the DeepGMG, GraphRNN and GNF for Ego-small and Community-small dataset are taken from their original papers.

Algorithm 5 Training Procedure of Guided GGFlow by Reinforcement Learning

Require: θ_0, θ, α, β, T, N_{steps}, traj, $G^0 \sim p_{\text{ref}}, u_t(G^t, G|G^1, G^0)$, T, N_{train}

$\theta \leftarrow \theta_0$
for $i \in \{1, \ldots, N_{\text{train}}\}$ **do**
  $\Delta t = 1/N_{\text{steps}}$
  Collect flow trajectory $\Big(G^0, t = 0, \mathcal{R}(G^0)\Big)$.
  for $n \in \{0, \ldots, N_{\text{steps}} - 1\}$ **do**
    $\hat{p}^V_{1|t}(V^1|V^t, V^0), \hat{p}^E_{1|t}(E^1|E^t, E^0), \mathbf{y} = \text{GraphEvo}(V^t, E^t, t)$
    Get $G^{t+\Delta t}$ by sampling from Equation 9.
    $(V^{t+\Delta t}, E^{t+\Delta t}) = G^{t+\Delta t}$
    $t = t + \Delta t$
    Compute the reward function $\mathcal{R}(G^{t+\Delta t})$.
    Collect flow trajectory $\Big(G^{t+\Delta t}, t + \Delta t, \mathcal{R}(G^{t+\Delta t})\Big)$.
  end for
  Update network using Equation 10.
  $t = 0$
end for
return Guided flow matching model θ^*

GraphAF (Shi et al., 2019) We follow the implementation guidelines provided in the TorchDrug tutorials (`https://torchdrug.ai/docs/tutorials/generation.html`).

GraphDF (Shi et al., 2019) Model scripts are sourced from the DiG repository (`https://github.com/divelab/DIG/tree/dig-stable/examples/ggraph/GraphDF`).

GraphVAE (Shi et al., 2019) Scripts are obtained from the GraphVAE section of the GraphRNN repository (`https://github.com/JiaxuanYou/graph-generation/tree/master/baselines/graphvae`).

MoFlow (Zang & Wang, 2020) Implementation scripts are taken from the MoFlow repository (`https://github.com/calvin-zcx/moflow`).

GraphEBM (Liu et al., 2021) We use the implementation available in the GraphEBM repository (`https://github.com/biomed-AI/GraphEBM`).

EDP-GNN (Niu et al., 2020) The model is implemented according to the scripts in the EDP-GNN repository (`https://github.com/ermongroup/GraphScoreMatching`).

GDSS (Jo et al., 2022b) Implementation details are sourced from the GDSS repository (`https://github.com/harryjo97/GDSS`).

GSDM (Luo et al., 2023) Scripts are implemented from the GSDM repository (`https://github.com/ltz0120/Fast_Graph_Generation_via_Spectral_Diffusion`).

PS-VAE (Kong et al., 2022) Implementation details are sourced from the PS-VAE repository (`https://github.com/THUNLP-MT/PS-VAE`).

MolHF (Zhu et al., 2023) The model is implemented according to the scripts in the MolHF repository (`https://github.com/violet-sto/MolHF`).

GRASP (Minello et al., 2024) Implementation details are sourced from the GRASP repository (`https://github.com/lcosmo/GRASP`).

SwinGNN (Yan et al., 2023) Implementation details are sourced from the SwinGNN repository (`https://github.com/DSL-Lab/SwinGNN`). The authors employ the 'gaussian_tv' MMD kernel, whereas other methods use 'gaussian_emd' or 'gaussian'. To ensure a fair comparison, we adopt the same kernel.

GruM (Jo et al., 2024) Scripts are implemented from the GruM repository (`https://github.com/harryjo97/GruM/`).

DiGress (Vignac et al., 2022) The implementation is based on the DiGress repository (`https://github.com/cvignac/DiGress`).

H.3 Details of Generic Datasets

H.3.1 Dataset

Ego-small This dataset consists of 200 small one-hop ego graphs derived from the Citeseer network (Sen et al., 2008). Each graph contains between 4 and 18 nodes.

Community-small This dataset includes 100 random community graphs, each formed by two communities of equal size generated using the E-R model (Erdős et al., 1960) with a probability parameter of $p = 0.7$. The graphs range in size from 12 to 20 nodes.

Enzymes The dataset comprises 587 protein graphs, with each graph representing the tertiary structure of enzymes sourced from the BRENDA database (Schomburg et al., 2004), which have between 10 and 125 nodes.

Grid The dataset consists of 100 standard 2D grid graphs with $100 \leq |V| \leq 400$.

Planar The dataset consists of 200 planar graphs, each with 64 nodes, generated using Delaunay triangulation on uniformly distributed random points.

Table S9: Statistics of the generic graph datasets

Dataset	type	Number of graphs	Number of nodes
Ego-small	Real	200	[4, 18]
Community-small	Synthetic	100	[12, 20]
Enzymes	Real	587	[10, 125]
Planar	Synthetic	200	64
Grid	Synthetic	100	[100,400]

H.4 Details of Molecule Datasets

H.4.1 Dataset

QM9 It is a subset of the GDB-17 database and consists of 134,000 stable organic molecules, each containing up to 9 heavy atoms: carbon, oxygen, nitrogen, and fluorine (Ramakrishnan et al., 2014). The dataset includes 12 tasks related to quantum properties. We follow the train/test split from GDSS, using 12,000 molecules for training and the remaining 1,000 for testing.

ZINC250k It contains 250,000 drug-like molecules with a maximum of 38 atoms per molecule (Irwin et al., 2012). It includes 9 atom types and 3 edge types. For a fair comparison, we use the same train/test split as previous works, such as GDSS and GSDM.

Table S10: Statistics of the molecular graph datasets

Dataset	type	Number of graphs	Number of nodes	Number of node types	Number of edge types
QM9	Real	133,885	[1, 9]	4	3
ZINC250k	Real	249,455	[6, 38]	9	3

H.4.2 Metrics

For generic graph datasets, we employ Maximum Mean Discrepancy (MMD) to assess the distributions of graph statistics, specifically degree distribution, clustering coefficient, the number of occurrences of 4-node orbits, and eigenvalues of the normalized graph Laplacian. In alignment with prior research (Jo et al., 2022b), we utilize specialized kernels for MMD calculations: the Gaussian Earth Mover's Distance (EMD) kernel for degree distribution and clustering coefficient, the Gaussian Total Variation (TV) kernel for eigenvalues of the normalized graph Laplacian, and a standard Gaussian kernel for the 4-node orbits. To ensure a fair comparison, the size of the prediction set matches that of the test set.

Validity We permit atoms to exhibit formal charges during valency checks because of the presence of formal charges in the training molecules. It is the fraction of valid molecules after valency correction or edge resampling.

Validity w/o correction This metric explicitly evaluates the quality of molecule generation before any correction phase, providing a baseline for raw generation performance.

FCD FCD quantifies the functional connectivity density within a molecule by computing distances and connectivity between atoms, based on both structural and chemical features. It describes the three-dimensional structure, topological features, and chemical properties of molecules, making it valuable in fields such as drug design, compound screening, and molecular simulations.

NSPDK NSPDK assesses molecular similarity by comparing shortest paths within their graphical structures. It captures connectivity patterns and chemical environments, effectively describing relationships and similarities between molecules. For two distributions p and q, the MMD using NSPDK is calculated as:

$$\mathrm{MMD}^2_{\mathrm{NSPDK}}(p,q) = \frac{1}{n(n-1)}\sum_{i=1}^{n}\sum_{j\neq i}^{n} k_{\mathrm{NSPDK}}(\mathcal{X}_i,\mathcal{X}_j) + \frac{1}{m(m-1)}\sum_{i=1}^{m}\sum_{j\neq i}^{m} k_{\mathrm{NSPDK}}(\mathcal{Y}_i,\mathcal{Y}_j) \tag{20}$$

$$- \frac{2}{mn}\sum_{i=1}^{n}\sum_{j=1}^{m} k_{\mathrm{NSPDK}}(\mathcal{X}_i,\mathcal{Y}_j) \tag{21}$$

Here, $k_{\mathrm{NSPDK}}(\cdot)$ denotes the NSPDK kernel function. $\mathcal{X}$ is the set of molecules from distribution p. $\mathcal{Y}$ is the set of molecules from distribution q. n and m represent the number of samples drawn from distributions p and q, respectively. This formula quantifies the difference between the distributions p and q using the NSPDK kernel.

H.5 Details of Conditional Generation

We included three guidance baselines in our conditional generation task:

DiGress model with guidance Utilizing the guidance method integrated into the DiGress model (Vignac et al., 2022).

Direct supervised training (ST) It involved selecting training samples from the dataset that satisfied $|\mu - \mu^*| < 1.0$ and retraining them using supervised learning settings identical to those in Section 4.2.

Supervised fine-tuning (SFT) This method involved fine-tuning a pre-trained GGFlow model on molecules generated with $|\mu - \mu^*| < 1.0$, maintaining the same training settings as in Section 4.2.

These models were trained over 10,000 steps using the training settings detailed in Section 4.2. We then generated 1,000 samples to calculate the results for each guidance method and the unconditional method, with the values of μ estimated using Psi4 (Smith et al., 2020). We set the hyperparameters α and β as 0.999 and 0.001.

I Experiment Settings

I.1 Hyperparameter Settings

Table S11 presents the hyperparameters employed in our experimental setup. For each dataset, the final resutls in Table 1 and Table 2 are the means of 5 different runs.

Table S11: Hyperparameter settings of different datasets

Hyperparameter	Ego-small	Community-small	Grid	Planar	Enzymes	QM9	ZINC250k
Number of layers	5	7	5	4	6	9	9
Hidden dimension of X	256	256	256	256	256	256	128
Hidden dimension of E	128	128	128	128	128	128	64
Hidden dimension of y	128	128	128	128	128	128	64
Optimizer	Adamw	Adamw	Adamw	Adamw	Adamw	Adamw	Adamw
Learning rate	2×10^{-4}	2×10^{-4}	2×10^{-4}	2×10^{-4}	2×10^{-4}	2×10^{-4}	2×10^{-4}
Batch size	64	128	4	64	8	512	128
Number of epochs	2000	3000	5000	5000	10000	1000	1000
Number of sampling steps	500	500	500	500	500	500	500

I.2 Ablation Studies Settings

For the evaluation of varying inference steps, we followed the same experimental settings as outlined in Sections 4.1 and 4.2. Samples were generated for 10 runs. The results were then visualized using the mean and variance across these 10 runs. It is important to note that in DiGress, the number of inference steps is constrained by its predefined diffusion steps ($N = 500$), so the DiGress curve terminates at 500 inference steps.

For the ablation studies of GGFlow without Optimal Transport (GGFlow w/o OT), GGFlow without GraphEvo (GGFlow w/o Evo) and GGFlow without GraphEvo and optimal transport (GGFlow w/o both), we adhered to the settings described in Sections 4.1 and 4.2. The final results were obtained by averaging the outcomes from five different runs.

Due to the excessive time required to compute metrics for 10,000 generated molecules, we conducted the experiments on inference steps and model stability using a smaller set of 1,000 generated molecules to calculate the test metrics on ZINC250k dataset.

To further investigate the advantages of optimal transport, we present generation results with varying inference steps on the Community-small dataset. As shown in Figure S3, GGFlow demonstrates superior generation quality compared to GGFlow (w/o OT), exhibiting narrower confidence intervals and comparable performance with fewer inference steps, which suggests that optimal transport enhances sampling both efficiency and stability.

I.3 Generation Times with Different Graph Scales

We conducted experiments to evaluate generation times across various graph scales using the Enzymes dataset. The GraphEvo model was configured with six layers, and generation time was measured for a single graph on an NVIDIA A100 80G GPU.

Table S12: Generation times with different graph scales.

Number of Nodes	10	50	100	200	400
Time (s)	1.92	4.24	12.15	48.59	235.8

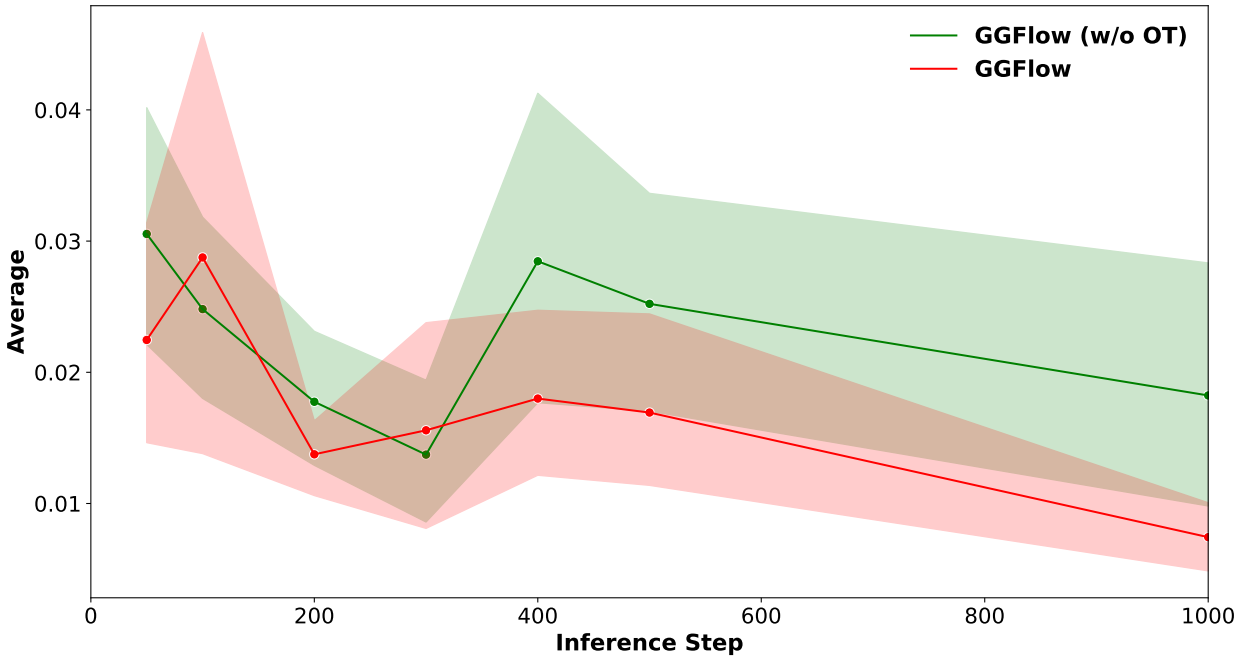

Figure S3: Ablation studies of varying inference steps on Community-small dataset

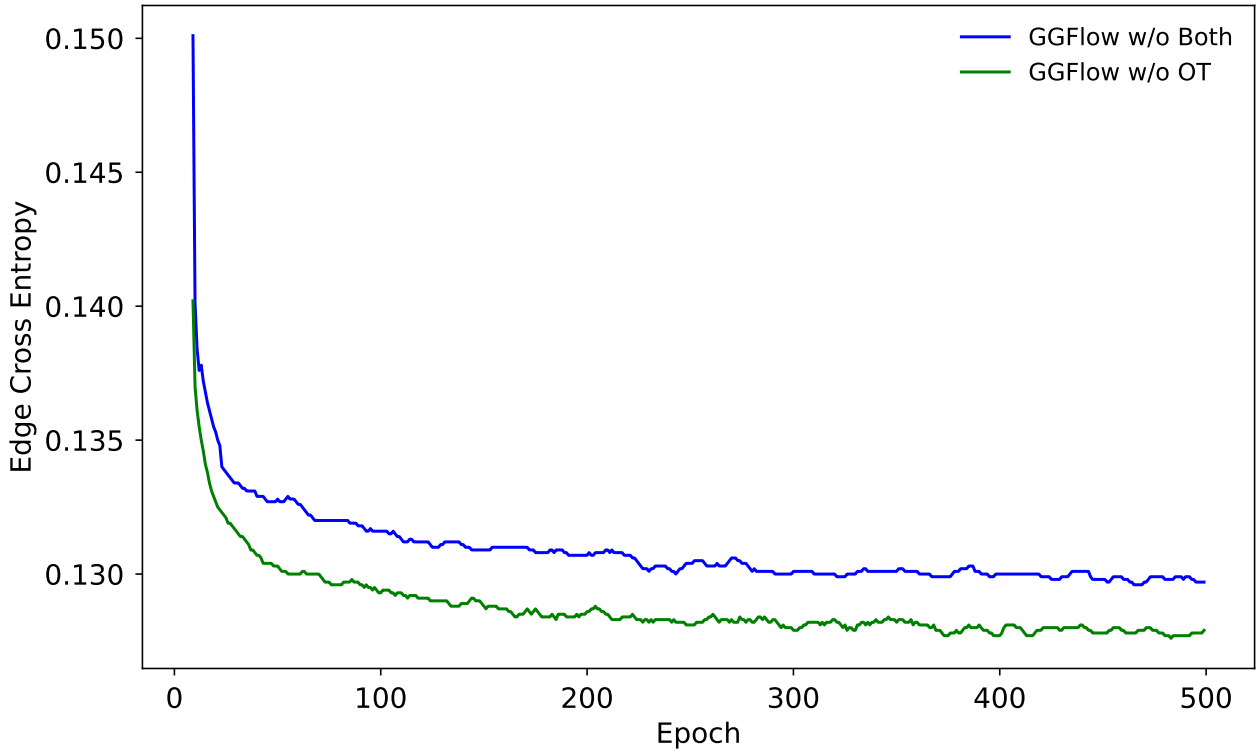

Figure S4: Cross-entropy of edges on the validation set for each epoch on ZINC250k dataset

J Visualization

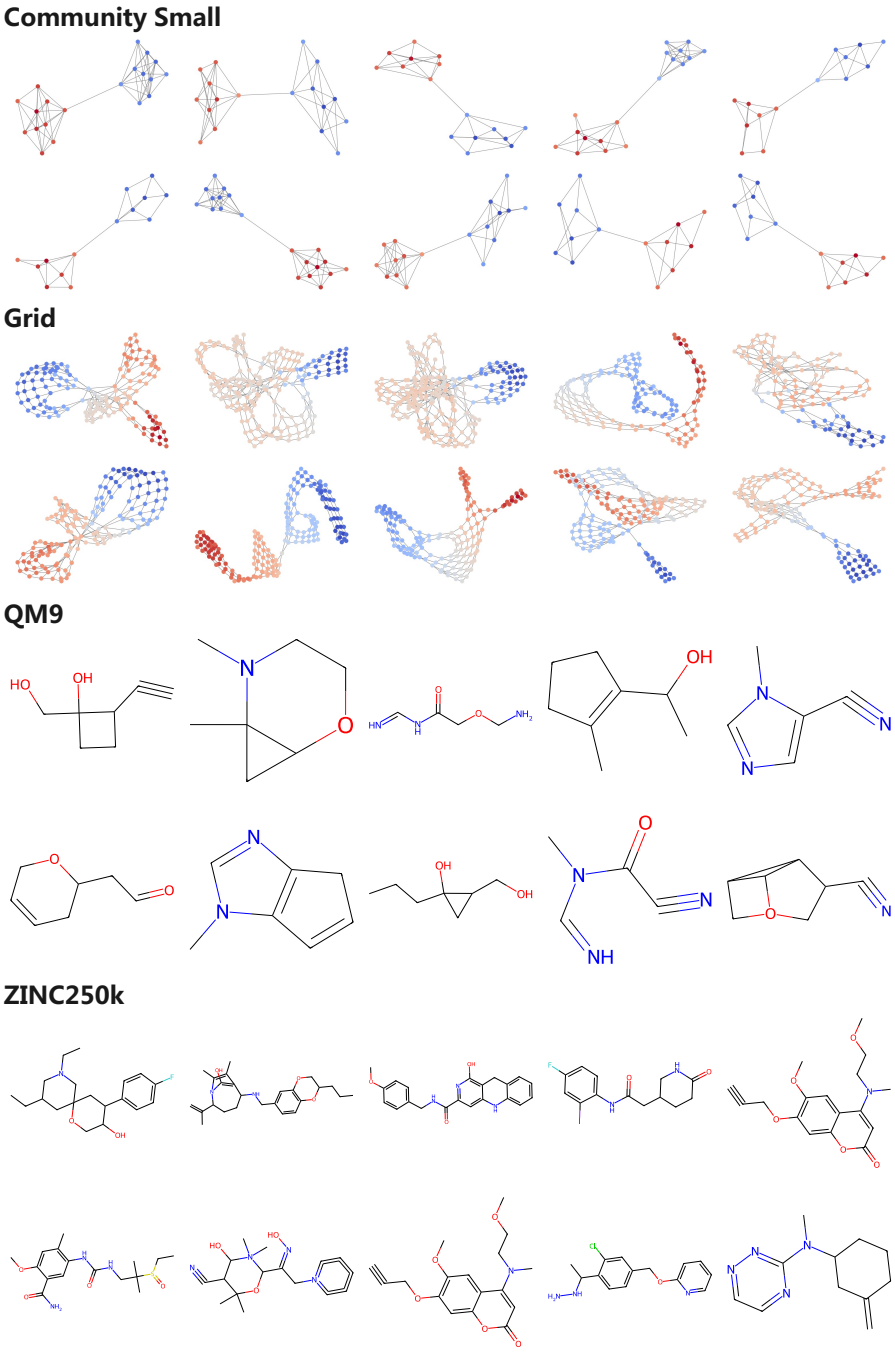

Figure S5: Visualization of generated samples of our model in different datasets